Gravitational Wave transient signal emission via Ekman Pumping in Neutron Stars during post-glitch relaxation phase

Avneet Singh[1, 2, 3, a, b]

[1] Max-Planck-Institut für Gravitationphysik, am Mühlenberg 1, 14476, Potsdam-Golm
[2] Max-Planck-Institut für Gravitationphysik, Callinstraβe 38, 30167, Hannover
[3] Leibniz Universität Hannover, Welfengarten 1, 30167, Hannover

Abstract

Glitches in the rotational frequency of a spinning neutron star could be promising sources of gravitational wave signals lasting between a few μs to a few weeks. The emitted signals and their properties depend upon the internal properties of the neutron star. In stellar models that assume a super-fluid core for the neutron star, the most important physical properties are the viscosity of the super-fluid, the stratification of flow in the equilibrium state and the adiabatic sound speed. Such models were previously studied by van Eysden and Melatos [26] and Bennett et al. [7] following simple assumptions on all contributing factors, in which the post-glitch relaxation phase could be driven by the well-known process of *Ekman pumping* [29, 2]. We explore the hydrodynamic properties of the flow of super-fluid during this phase following more relaxed assumptions on the stratification of flow and/or the pressure-density gradients within the neutron star than previously studied. We calculate the time-scales of duration as well as the characteristic strengths of the resulting gravitational wave signals, and we detail their dependence on the physical properties of the super-fluid core. We find that it is possible for the neutron star to emit gravitational wave signals in a wide range of decay time-scales and within the detection sensitivity of aLIGO for selected domains of physical parameters.

1 Introduction

Pulsar glitches are sudden fractional increases in the rotational velocity of a neutron star. Several pulsars, observed in radio, X-ray and γ-ray bands of the electromagnetic spectrum, have been repeatedly observed to glitch [9, 30, 12]. The fractional spin-up $\delta\Omega$ of the rotational velocity Ω of the neutron star lies in the range of $\frac{\delta\Omega}{\Omega} \in [O(10^{-11}), O(10^{-4})]$[26, 12, 18].

Gravitational wave emission is associated with a typically non-zero derivative of the quadrupole moment stemming from accelerated flow of non-axisymmetrically distributed bulk of matter. It is possible that such non-axisymmetric motions are excited following a glitch; possible mechanisms for producing such non-axisymmetric motions include bulk two-stream instabilities [5], surface two-stream instabilities [13], crust deformation and precession [10], meridional circulation and super-fluid turbulence driven by crust-core differential rotation [20], excitation of pulsation modes [21, 22, 23]. The aforementioned mechanisms have been briefly reviewed by van Eysden and Melatos [26] and Bennett et al. [7]. In general, a glitch can lead to gravitational waves emission in two phases. Initially, a burst-type emission occurs during the fast spin-up of crust at time-scales of at most a few seconds [15]. Secondly, a decaying continuous-wave signal during the post-glitch relaxation phase is emitted on much longer time scales. The initial non-axisymmetric motion of the bulk with respect to the crust in the second case is excited by the glitch. The resulting damped continuous-wave-like signal arises as the internal super-fluid dynamics evolve to set the bulk in co-rotation or a steady differential rotation with the crust, erasing the non-axisymmetric motions in the bulk super-fluid [26, 7].

In this paper, we consider the emission of gravitational waves during the post-glitch relaxation phase via the mechanism of *Ekman pumping* and related processes that precede and follow it, pioneered by Walin [29] and Abney and Epstein [2]. We extend the previous works on this by van Eysden and Melatos [26] and Bennett et al. [7], where an initial non-axisymmetric perturbation introduced by the glitch induces *Ekman pumping* in the core of the star. *Ekman pumping* is briefly described as the induced flow of the overall bulk matter when the bulk matter is acted upon by a tangential force (in this case, Coriolis force) at its boundary i.e. the crust-core interface. In our case, the Coriolis force results from the differential rotation of the crust from the bulk super-fluid, arising from the glitch in the star's rotational velocity. This induced flow of the bulk matter could then have a time-varying quadrupole moment and lead to emission of gravitational waves. We relax certain assumptions in more recent works [26, 7] on the stratification length and the adiabatic sound speed; we explore a regime of *Ekman pumping* where these quantities are allowed to vary across the star and study their effect on the emitted gravitational wave signal. This extends the parameter space as well as the considered ranges of values of the physical parameters, and introduces more generality to the analysis.

[a] avneet.singh@aei.mpg.de
[b] avneet.singh@ligo.org

We will keep the simplifying assumptions made in [2, 26], and analyze the system in a pure hydrodynamical sense, ignoring the two-stream dynamics, sidestepping the crust-core interface, neglecting the effects of pinning and unpinning of quantum vortices, and disallowing the crust to precess. Moreover, for analytic simplicity, we approximate our spherical neutron star to a fluid-filled rigid cylinder [7], as opposed to the choice of semi-rigidity [26]. The correctness of this choice will be explained in the next section. In nutshell, as a result of all these simplifications, a simplified toy-model for a neutron star is studied for the possibility of emission of gravitational waves.

2 Hydrodynamics of the system

Let us consider a rotating neutron star of radius of order O(L) with a solid crust around a compressible and viscous super-fluid with viscosity ν, pressure p and density ρ. We now approximate this spherical system with a rigid cylindrical container of height 2L and radius L rotating at an angular frequency of Ω along the z-axis (figure 1). We represent the glitch as a sudden perturbation in the angular velocity of magnitude $\delta\Omega$ along the z-axis. This geometric simplification doesn't lead to an order-of-magnitude change in the strength of the emitted gravitational wave signal from *Ekman pumping* [27], and has historically been used in majority of literature on neutron star modeling. Moreover, this reformulation to the cylindrical system leads to simpler analytically solvable solutions.

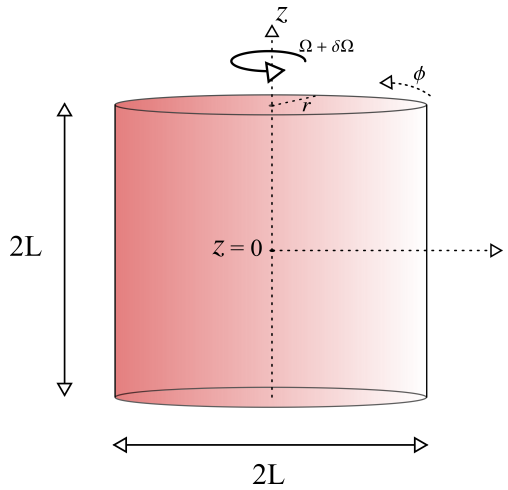

Figure 1: Idealized system

2.1 Governing equations

Our physical system is described by the velocity field $\vec{v}$, the pressure p and the density ρ of the fluid. The forces acting on fluid elements of the bulk volume are the viscous force, the Coriolis force, the centrifugal force, the compressible strain, pressure gradients and gravitational force. The Navier-Stokes equation, the conservation of mass equation, and the 'energy equation' (i.e. equation of state) govern our physical system. The Navier-Stokes equation for a fluid element in the rotating Lagrangian frame of the cylinder for a compressible fluid is given by

$$\frac{\partial \vec{v}}{\partial t} + \vec{v}\cdot\boldsymbol{\nabla}\vec{v} + 2\vec{\Omega}\times\vec{v} = -\frac{1}{\rho}\boldsymbol{\nabla}p + \nu\,\boldsymbol{\nabla}^2\vec{v} + \frac{\nu}{3}\boldsymbol{\nabla}(\vec{\boldsymbol{\nabla}}\cdot\vec{v}) + \boldsymbol{\nabla}[\Omega\times(\Omega\times r)] + \vec{g} \tag{1}$$

where, $\vec{v}$ is the fluid velocity and $\vec{g}$ is the gravitational acceleration. The Navier-Stokes equation relates the restoring forces on a fluid element (written on the right-hand side; pressure gradients, viscous force, gravitational force, compressible strain, centrifugal force) to the impulsive change in momentum of the fluid element (written on the left-hand side; Coriolis force etc). We have ignored terms from the magnetic field of the neutron star for the sake of simplicity, restricting ourselves to a purely hydrodynamical analysis. The gravitational acceleration is taken to be of the following form:

$$\vec{g} = -\frac{z}{|z|}g\hat{z}. \tag{2}$$

This form for $\vec{g}$ is unphysical since it appears to be generated by a singular planer mass distribution located at $z = 0$. However, such a choice is standard in neutron star literature [2, 26]; it leads to an analytically solvable set of equations which compare well to numerical simulations comprising of smoother and more realistic mass distributions [19]. This assumption further incorporates symmetrical flow across the mid-plane of the cylinder so that we can restrict the analysis to the domain $z \geq 0$.

The second governing equation is the 'Continuity Equation', or alternatively, the conservation of mass equation

$$\frac{\partial \rho}{\partial t} + \boldsymbol{\nabla}\cdot(\rho\vec{v}) = 0 \tag{3}$$

Lastly, we write the 'energy equation' (in principle, the general classical equation of state) in terms of the adiabatic sound speed v_c (where, the sub-script S represents derivative taken at constant entropy) of the form[1]

$$\left[\frac{\partial p}{\partial \rho}\right]_S = v_c^2 \quad \text{or,} \quad \rho = \frac{p}{v_c^2} \tag{4}$$

which in a Lagrangian frame (also known as 'convective derivative form') takes the following form,

$$\left[\frac{\partial}{\partial t} + \vec{v}\cdot\boldsymbol{\nabla}\right]\rho = \left[\frac{\partial}{\partial t} + \vec{v}\cdot\boldsymbol{\nabla}\right]\frac{p}{v_c^2} \tag{5}$$

[1] We choose the most general form for the equation of state upon integration and set the constant of integration to 0.

Note that we do not impose invariance of v_c in either space or time as previously done in [26, 7].

Now, we scale our variables to dimensionless form by redefining them as, $r \to \mathrm{L}r$, $z \to \mathrm{L}z$, $\vec{v} \to (\delta\Omega)\mathrm{L}\vec{v}$, $\rho \to \rho_o\rho$, $p \to \rho_o g\mathrm{L}p$, $\boldsymbol{\nabla} \to \mathrm{L}^{-1}\boldsymbol{\nabla}$, $t \to t_e t$; where we define ρ_o as the equilibrium mass-density at $z = 0$, and t_e and the *Ekman number* E as,

$$t_e = \mathsf{E}^{\frac{1}{2}}\Omega^{-1}, \quad \text{and, } \mathsf{E} = \frac{\nu}{\mathrm{L}^2\Omega} \tag{6}$$

One can then write the governing equations (1), (3) and (5) in the re-scaled form as

$$\epsilon\mathsf{F}\left[\mathsf{E}^{\frac{1}{2}}\frac{\partial\vec{v}}{\partial t} + \epsilon\vec{v}\cdot\boldsymbol{\nabla}\vec{v} + 2\hat{e}_z\times\vec{v}\right] = -\frac{1}{\rho}\boldsymbol{\nabla}p - \vec{e}_z + \epsilon\mathsf{F}\mathsf{E}\left[\boldsymbol{\nabla}^2\vec{v} + \frac{1}{3}\boldsymbol{\nabla}\{\boldsymbol{\nabla}\cdot\vec{v}\}\right] + \mathsf{F}\boldsymbol{\nabla}\left[\frac{1}{2}r^2\right] \tag{7}$$

$$\mathsf{E}^{\frac{1}{2}}\frac{\partial\rho}{\partial t} + \epsilon\boldsymbol{\nabla}\cdot(\rho\vec{v}) = 0 \tag{8}$$

$$\mathsf{E}^{\frac{1}{2}}\frac{\partial[\rho\eta]}{\partial t} + \epsilon\vec{v}\cdot\boldsymbol{\nabla}[\rho\eta] = \mathsf{K}\left[\mathsf{E}^{\frac{1}{2}}\frac{\partial p}{\partial t} + \epsilon\vec{v}\cdot\boldsymbol{\nabla}p\right] \tag{9}$$

where η, the *Froude number* F, the maximum *scaled compressibility* K, and the *Rossby number* ϵ are defined as

$$\eta = \frac{v_c^2}{c^2}, \quad \mathsf{K} = g\frac{\mathrm{L}}{c^2}, \quad \mathsf{F} = \Omega^2\frac{\mathrm{L}}{g}, \quad \epsilon = \frac{\delta\Omega}{\Omega} \tag{10}$$

2.2 Orders of magnitude

We list the physical constants and parameters introduced in the previous section, and their order-of-magnitude values in SI units for the interior of a neutron star from general estimates on the known physical properties of such a system:

$$g = O(10^{12}),\ \mathrm{L} = O(10^4),\ \frac{\Omega}{2\pi} = O(1\mathrm{Hz} - 10^2\mathrm{Hz}),\quad \mathsf{E} \in [O(10^{-17}), O(10^{-7})],\ \frac{v_c}{c} \in [O(10^{-2}), 1] \tag{11}$$

The viscosity ν of the super-fluid for a neutron star is currently unknown and widely debated. The associated value of *Ekman number* E also remains volatile. Yet, there are estimates on the value of E from results of heavy-ion collision experiments [26, 3, 14, 4, 11] and from theoretical calculations of neutron-neutron scattering in a super-fluid [8, 16]. The results from such analysis lead to the wide range of possible values for E quoted above in (11). The secondary parameters in (10) then take the following values[2]

$$\mathsf{K} = O(10^{-1}),\quad \mathsf{F} \in [O(10^{-9}), O(10^{-3})],\quad \epsilon \in [O(10^{-11}), O(10^{-4})] \tag{12}$$

3 Solution

We present the solutions to the governing equations given in the section 2.1.

3.1 Equilibrium solution

In equilibrium, due to the symmetry of the system across the $z = 0$ mid-plane and the time-invariance of involved forces specified in (1), the flow is steady and axisymmetric, and the density and pressure are functions of z and r only. Since ϵ and F are quite small in their absolute magnitude, we can ignore the centrifugal term [2] in the re-scaled equations (7), (8) and (9). With this approximation, (7) reduces to

$$\frac{1}{\rho}\boldsymbol{\nabla}p + \vec{e}_z = 0 \tag{13}$$

In order to solve the above equation, we need to make a simplifying assumption for either the mass-density or the pressure. We reformulate the introduction of the dimensionless parameter $\mathsf{K_s}$ in [26] and assume the following:

$$\rho^{-1}(\mathrm{d}\rho/\mathrm{d}z) = -\mathsf{K_s}(z) \tag{14}$$

We define the stratification length z_s in terms of the dimensionless quantity $\mathsf{K_s}$ as $z_s = \mathrm{L}\,\mathsf{K_s}^{-1}$. The above expression is essentially an assumed steady-state density profile of the system. The equilibrium pressure and density profiles are then given by solving (13) and (14) respectively,

$$\rho_e(z) = e^{-\int_0^z \mathsf{K_s}(z')\,\mathrm{d}z'} \tag{15}$$

$$p_e(z) = \mathsf{K_s}^{-1}(z)\,e^{-\int_0^z \mathsf{K_s}(z')\,\mathrm{d}z'} \tag{16}$$

Here, we have not assumed $\mathsf{K_s}$ to be a constant as previously done in [26, 7]. The introduction of the form $\mathsf{K_s}$ is not trivial. In fact, the assumption of a certain form of $\mathsf{K_s}$ incorporates the nature of entropic or compositional gradients, which in turn incorporate the digression of equilibrium state from an adiabatic state. One could introduce *equilibrium sound speed* accordingly, given by $v_{\mathrm{eq}}^2 = \dfrac{g\mathrm{L}}{\mathsf{K_s}(z)}$. It must be noted that in equilibrium state, the gravity acts to vary density (and subsequently pressure) along the axis of the cylinder in z-direction.

3.2 Induced Perturbations

Let us assume that a glitch induces perturbations in pressure, density and velocity fields of the internal bulk fluid of the neutron star and the resultant bulk fluid flow/motion may be non-axisymmetric in nature. When such perturbations are induced by a glitch, the density $\rho(r, \phi, z, t)$ and pressure $p(r, \phi, z, t)$ then take all spatial

[2] We will use the values quoted in (11) and (12) when making order-of-magnitude estimates on the emitted gravitational wave signals.

and temporal coordinates as arguments in addition to the z-coordinate, as opposed to the case of stable equilibrium. In order to solve for the evolved fluid motion, we treat the system perturbatively given the small magnitude of ϵ. In such a scenario, the density, pressure and the velocity field can be expanded as $\rho \rightarrow \rho + \epsilon\delta\rho$, and $p \rightarrow p + \epsilon\delta p$, where we have let the magnitude of δp and $\delta\rho$ run free and normalized it to its nominal value by ϵ. The velocity field, however, is written simply as $\vec{v} \rightarrow \delta\vec{v}$. We do not perturb η explicitly; the variation in η will arise naturally from variation in v_c. Now, ignoring all terms larger then $O(1)$ in ϵ, the set of 3 scaled governing equations (7), (8) and (9) then reduce to

$$\mathsf{F}\left[\mathsf{E}^{\frac{1}{2}}\frac{\partial[\delta\vec{v}]}{\partial t} + 2\hat{e}_z \times [\delta\vec{v}]\right] = -\frac{1}{\rho}\boldsymbol{\nabla}[\delta p] - \frac{\delta\rho}{\rho}\vec{e}_z + \mathsf{F}\,\mathsf{E}\left[\boldsymbol{\nabla}^2[\delta\vec{v}] + \frac{1}{3}\boldsymbol{\nabla}\{\boldsymbol{\nabla}\cdot[\delta\vec{v}]\}\right] + \mathsf{F}\frac{\delta\rho}{\rho}\boldsymbol{\nabla}\left[\frac{1}{2}r^2\right] \tag{17}$$

$$\mathsf{E}^{\frac{1}{2}}\frac{\partial[\delta\rho]}{\partial t} + \boldsymbol{\nabla}\cdot(\rho\,\delta\vec{v}) = 0 \tag{18}$$

$$\mathsf{E}^{\frac{1}{2}}\frac{\partial[\eta\delta\rho]}{\partial t} + \delta\vec{v}\cdot\boldsymbol{\nabla}[\rho\eta] = \mathsf{K}\left[\mathsf{E}^{\frac{1}{2}}\frac{\partial[\delta p]}{\partial t} + \delta\vec{v}\cdot\boldsymbol{\nabla}p\right] \tag{19}$$

3.3 Method of multiple scales

We now employ the method of multiple scales which has been previously used in [26, 7, 29, 2]. The perturbations in the density, pressure and velocity field can now be expanded into scales of order E^0, $\mathsf{E}^{\frac{1}{2}}$ and E^1, such that for density perturbations

$$\delta\rho = \delta\rho^{(0)} + \mathsf{E}^{\frac{1}{2}}\delta\rho^{(1)} + \mathsf{E}^1\delta\rho^{(2)} \tag{20}$$

and for pressure perturbations,

$$\delta p = \delta p^{(0)} + \mathsf{E}^{\frac{1}{2}}\delta p^{(1)} + \mathsf{E}^1\delta p^{(2)} \tag{21}$$

and for velocity perturbations,

$$\delta\vec{v} = \delta\vec{v}^{(0)} + \mathsf{E}^{\frac{1}{2}}\delta\vec{v}^{(1)} + \mathsf{E}^1\delta\vec{v}^{(2)} \tag{22}$$

The idea behind breaking down the perturbations scale-wise is that the governing equations at discretised scales at increments of $\mathsf{E}^{\frac{1}{2}}$ are analytically solvable.

One can now solve (17) for the the velocity field i.e. its radial, azimuthal and vertical components of $v_r^{(i)}$, $v_\phi^{(i)}$ and $v_z^{(i)}$ up to ith order in $\mathsf{E}^{\frac{i}{2}}$,

$$\mathsf{F}\left[\mathsf{E}^{\frac{1}{2}}\frac{\partial\delta v_r}{\partial t} - 2\delta v_\phi\right] = -\frac{\partial}{\partial r}\left[\frac{\delta p}{\rho}\right] + \mathsf{F}\mathsf{E}\times \left[\left\{\boldsymbol{\nabla}^2 - \frac{1}{r^2}\right\}\delta v_r - \frac{2}{r^2}\frac{\partial[\delta v_\phi]}{\partial\phi} + \frac{1}{3}\frac{\partial}{\partial r}[\boldsymbol{\nabla}\cdot\delta\vec{v}]\right] \tag{23}$$

$$\mathsf{F}\left[\mathsf{E}^{\frac{1}{2}}\frac{\partial\delta v_\phi}{\partial t} - 2\delta v_r\right] = -\frac{1}{r}\frac{\partial}{\partial\phi}\left[\frac{\delta p}{\rho}\right] + \mathsf{F}\mathsf{E}\times \left[\left\{\boldsymbol{\nabla}^2 - \frac{1}{r^2}\right\}\delta v_\phi - \frac{2}{r^2}\frac{\partial[\delta v_r]}{\partial\phi} + \frac{1}{3r}\frac{\partial}{\partial\phi}[\boldsymbol{\nabla}\cdot\delta\vec{v}]\right] \tag{24}$$

$$\mathsf{F}\mathsf{E}^{\frac{1}{2}}\frac{\partial\delta v_z}{\partial t} = -\frac{1}{\rho}\frac{\partial}{\partial z}\left[\frac{\delta p}{\rho}\right] - \frac{\delta\rho}{\rho} + \mathsf{F}\mathsf{E}\times \left[\boldsymbol{\nabla}^2[\delta v_z] - \frac{1}{3}\frac{\partial}{\partial\phi}[\boldsymbol{\nabla}\cdot\delta\vec{v}]\right] \tag{25}$$

Two additional relations are derived from the energy equation (19) and the continuity equation (18), and they are given by

$$\mathsf{E}^{\frac{1}{2}}\frac{\partial}{\partial t}\left[\frac{\delta\rho}{\rho}\right] + \boldsymbol{\nabla}\cdot\delta\vec{v} = \mathsf{K}_\mathsf{s}(z)\delta v_z \tag{26}$$

and,

$$\eta(z)\mathsf{E}^{\frac{1}{2}}\frac{\partial}{\partial t}\left[\frac{\delta\rho}{\rho}\right] = \mathsf{K}\mathsf{E}^{\frac{1}{2}}\frac{\partial}{\partial t}\left[\frac{\delta p}{\rho}\right] + \mathsf{F}\mathsf{N}^2(z)\,\delta v_z \tag{27}$$

where, we have introduced $\mathsf{N}(z)$ - the re-normalized *Brunt-Väisälä frequency*[3]:

$$\mathsf{N}^2(z) = \frac{[\eta\mathsf{K}_\mathsf{s} - \partial_z\eta] - \mathsf{K}}{\mathsf{F}} = \frac{\mathsf{K}}{\mathsf{F}}\left[\frac{v_c^2}{v_{eq}^2} - 1\right] - \frac{\partial_z\eta}{\mathsf{F}} \tag{28}$$

We can reformulate (28) by introducing $\mathsf{K}'_\mathsf{s}(z)$:

$$\mathsf{K}'_\mathsf{s}(z) = \eta\mathsf{K}_\mathsf{s} - \partial_z\eta = \mathsf{K}\frac{v_c^2}{v_{eq}^2} - \partial_z\eta \tag{29}$$

such that (28) takes the simpler following form:

$$\mathsf{N}^2(z) = \frac{\mathsf{K}'_\mathsf{s}(z) - \mathsf{K}}{\mathsf{F}} \tag{30}$$

where, η and K_s are allowed to vary with z only. In the set of equations (23)-(27), one can see the terms on all $O(\mathsf{E}^0)$, $O(\mathsf{E}^{\frac{1}{2}})$ and $O(\mathsf{E}^1)$ scales. Thus, the equations (23)-(27) are now easily reducible at each order. Moreover, one can now effectively distinguish and deduce the time-scales at which several processes contribute to the overall perturbed flow of the bulk matter, such as the formation of viscous *Rayleigh shear layer* layer, followed by partial spin-up of the interior fluid via *Ekman pumping*, followed by complete spin-up of the interior on longer time-scales. These processes have been discussed briefly by van Eysden and Melatos [26] and in much greater detail by Abney and Epstein [2]. We will also discuss them in the later section(s). These times scales are naturally: $\mathsf{E}^0\Omega^{-1}$, $\mathsf{E}^{-\frac{1}{2}}\Omega^{-1}$ and $\mathsf{E}^{-1}\Omega^{-1}$. One can now isolate solutions at these different scales since they become effectively independent owing to very small values of the *Ekman number* E.

[3]Note that the re-normalised *Brunt-Väisälä frequency* $\mathsf{N}(z)$ is a well-known quantity in fluid mechanics and atmospheric sciences. It is a measure of the buoyant force experienced by a fluid element when displaced from equilibrium.

3.4 $O(\mathsf{E}^0)$ solutions

To the order of E^0, the expressions (23)-(27) reduce to

$$\delta v_r^{(0)} = -\frac{1}{2\mathsf{F}r}\frac{\partial}{\partial\phi}\left[\frac{\delta p^{(0)}}{\rho}\right] \tag{31}$$

$$\delta v_\phi^{(0)} = \frac{1}{2\mathsf{F}}\frac{\partial}{\partial r}\left[\frac{\delta p^{(0)}}{\rho}\right] \tag{32}$$

$$\delta v_z^{(0)} = 0 \tag{33}$$

$$\delta\rho^{(0)} = -\frac{\partial[\delta p^{(0)}]}{\partial z} \tag{34}$$

$$\boldsymbol{\nabla}\cdot\delta\vec{v}^{(0)} = 0 \tag{35}$$

Note that the solutions up to order E^0 are exactly similar to the ones previously achieved in [26, 7, 29, 2]. These solutions, given by (31)-(35), correspond to the formation of a viscous boundary layer (also referred to as simply the *Rayleigh shear layer*) on the top and bottom faces of the cylinder on a time-scale $O(\mathsf{E}^0\Omega^{-1})$. Within this viscous boundary layer, the flow tends to move radially due to the gradient in the azimuthal velocity, and the resulting imbalance between centrifugal and pressure gradient forces [29, 2].

3.5 $O(\mathsf{E}^{\frac{1}{2}})$ solutions

In order to get the $O(\mathsf{E}^{\frac{1}{2}})$ solutions, we assume for simplicity that

$$\frac{\delta p^{(1)}}{p} = \frac{\delta\rho^{(1)}}{\rho} \equiv 0 \tag{36}$$

The $O(\mathsf{E}^{\frac{1}{2}})$ reductions to (23)-(27) then respectively yield

$$\delta v_r^{(1)} = \frac{1}{4\mathsf{F}}\frac{\partial\chi}{\partial r} \tag{37}$$

$$\delta v_\phi^{(1)} = \frac{1}{4\mathsf{F}r}\frac{\partial\chi}{\partial\phi} \tag{38}$$

$$\delta v_z^{(1)} = \frac{\eta(z)}{\mathsf{F}\mathrm{N}^2(z)}\frac{\partial\chi}{\partial z} + \left[\frac{-\partial_z\eta}{\mathsf{F}\mathrm{N}^2(z)} - 1\right]\chi \tag{39}$$

$$\frac{\partial}{\partial t}\left[\frac{\delta\rho^{(0)}}{\rho}\right] + \boldsymbol{\nabla}\cdot\delta\vec{v}^{(1)} = \mathsf{K_s}(z)\delta v_z^{(1)} \tag{40}$$

where, we have defined χ as

$$\chi = -\frac{\partial}{\partial t}\left[\frac{\delta p^{(0)}}{\rho}\right] \equiv O(\mathsf{E}^0) \tag{41}$$

These set of solutions represent the core process of *Ekman pumping* - the flow in the viscous boundary layer, given by (31)-(35), sets a secondary motion in the interior[4]; the fluid is pulled into the viscous boundary layer to replace the radial outward flow from the boundary layer [29, 2]. Note that the results at the order $O(\mathsf{E}^{\frac{1}{2}})$, given by (37)-(40), are markedly different from previous works with respect to the expressions for $\delta v_z^{(1)}$ in (39) as well as for the reduced continuity equation (40). This will affect all future calculations as we will further see.

3.6 More on the scale-based solutions

We will skip the discussion of the $O(\mathsf{E}^1)$ solutions since they occur at much larger time-scales of $O(\mathsf{E}^{-1}\Omega^{-1})$, and correspond to the eventual 'spin-up' of the entire interior bulk matter. This eventual 'spin-up' refers to the final state of the system when the interior bulk sets in complete co-rotation or steady differential co-rotation with the crust, as previously mentioned [29, 2]. Such processes at large time-scales are irrelevant to our discussion since they do not relate to the processes that contribute to the gravitational wave emission. Reiterating the discussion in previous sections, the sudden spin-up of the rotating cylinder leads to the formation of a viscous boundary layer at the top and bottom of the rotating cylinder. This viscous layer forms on a time-scale of $O(\mathsf{E}^0\Omega^{-1})$. The velocity field within the layer then pushes the fluid radially through the layer given by (31)-(33). The $O(\mathsf{E}^0)$ flow then excites the secondary process of *Ekman pumping* in the interior on a time scale of $O(\mathsf{E}^{-\frac{1}{2}}\Omega^{-1})$, part of it vertically into the viscous boundary layer given by (37)-(39). One can see that the vertical velocity in this case is non-zero. This vertical velocity is constrained by the continuity law applied to the viscous layer [2, 26, 29], such that

$$\delta v_z|_{z=\pm1} = \pm\frac{1}{2}\mathsf{E}^{\frac{1}{2}}(\boldsymbol{\nabla}\times\delta\vec{v})_z|_{z=\pm1} \tag{42}$$

The above expression describes the vertical flow across and into the viscous layer as a function of flow just outside the layer on a time scale of $O(\mathsf{E}^{\frac{1}{2}})$, apparent in the magnitude of the accompanying coefficient. We here assume that the boundary layer is fully co-rotating with the cylinder at frequency Ω following the assumption of rigidity. However, if one takes into account the slippage of the boundary layer relative to the container across the top and bottom faces, this assumption doesn't hold true. In such a scenario, the term $\delta\vec{v}$ must be replaced with $\delta\vec{v} - \vec{v}_\mathsf{B}$, where $\vec{v}_\mathsf{B}$ is the dimensionless relative velocity of the boundary layer given by $r\vec{e}_\phi$ [7]. We will forgo this factor of $\vec{v}_\mathsf{B}$ and assume a co-rotating viscous boundary layer; it only leads to a redundant renormalization which is essentially irrelevant to the gravitational wave emission characteristics. *Ekman pumping* eventually stops when $\delta\vec{v} = 0$, followed up by spin-up of the entire interior on time-scales $O(\mathsf{E}^{-1}\Omega^{-1})$. On the other hand, in presence of $\vec{v}_\mathsf{B}$, *Ekman pumping* stops when $\delta\vec{v} = \vec{v}_\mathsf{B}$. Furthermore, the magnitude term of $\mathsf{E}^{\frac{1}{2}}$ can be understood in terms of scaling arguments; see the

[4] The important development is the excitation of flow in z-direction, given by (39).

detailed discussion by Abney and Epstein [2]. The viscous term in the dimensionless Navier-Stokes equation (7) is given by

$$\mathsf{FE}\boldsymbol{\nabla}^2 \rightarrow \mathsf{FE}\left[\frac{1}{\delta \mathrm{L}}\right]^2 \equiv O(\mathsf{F}) \tag{43}$$

where, $\delta\mathrm{L}$ is the characteristic scale of the thickness of the viscous layer. Clearly, from the given relation above, $\delta\mathrm{L} = O(\mathsf{E}^{\frac{1}{2}})$.

3.7 The characteristic equation

Considering the $O(\mathsf{E}^0)$ and $O(\mathsf{E}^{\frac{1}{2}})$ solutions obtained in the previous sections, they can now be combined to give the following singular differential equation with terms up to order $O(\mathsf{E}^{\frac{1}{2}})$ and $O(\mathsf{F}^0)$:

$$\frac{1}{r}\frac{\partial}{\partial r}\left[r\frac{\partial \chi}{\partial r}\right] + \frac{1}{r^2}\frac{\partial^2 \chi}{\partial \phi^2} - \left[\frac{4\eta(z)\mathsf{K_s}(z)}{\mathsf{N}^2(z)}\right]\frac{\partial \chi}{\partial z} + \frac{4\eta(z)}{\mathsf{N}^2(z)}\frac{\partial^2 \chi}{\partial z^2} = \left[\frac{\partial_z \eta - \partial_z^2 \eta}{\mathsf{N}^2(z)}\right]\chi \tag{44}$$

The above characteristic equation can be solved via the standard *method of separation of variables* to yield

$$\chi(r,\phi,z,t) = \sum_{\alpha=0}^{\infty}\sum_{\gamma=1}^{\infty} \mathsf{J}_\alpha(\lambda_{\alpha\gamma} r)\left[\frac{\mathrm{A}_{\alpha\gamma}(t) - i\mathrm{B}_{\alpha\gamma}(t)}{2} \times e^{i\alpha\phi} + \frac{\mathrm{A}_{\alpha\gamma}(t) + i\mathrm{B}_{\alpha\gamma}(t)}{2} e^{-i\alpha\phi}\right]\mathrm{Z}_{\alpha\gamma}(z) \tag{45}$$

where, $\lambda_{\alpha\gamma}$ is the γth zero of the αth Bessel mode (J_α), and $\mathrm{A}_{\alpha\gamma}(t)$, $\mathrm{B}_{\alpha\gamma}(t)$ are the associated *Bessel-Fourier coefficients* which depend upon the assumed steady-state solution, as we will see shortly. The flow is constrained by a trivial boundary condition which requires no penetration through the side walls, i.e. $\delta v_r^{(0)}|_{r=1} = 0$. This simply translates to $\partial_\phi \chi|_{r=1} = 0$ for all ϕ, via (31). Moreover, $\mathrm{Z}_{\alpha\gamma}(z)$ is the solution to the following differential equation,

$$\frac{4\eta(z)}{\mathsf{N}^2(z)}\frac{\partial^2 \mathrm{Z}_{\alpha\gamma}(z)}{\partial z^2} - \frac{4\eta(z)\mathsf{K_s}(z)}{\mathsf{N}^2(z)}\frac{\partial \mathrm{Z}_{\alpha\gamma}(z)}{\partial z} - \left[\frac{\partial_z \eta - \partial_z^2 \eta}{\mathsf{N}^2(z)} + \lambda_{\alpha\gamma}^2\right]\mathrm{Z}_{\alpha\gamma}(z) = 0 \tag{46}$$

which clearly depends on N^2, which is turn depends exclusively on $\mathsf{K_s}$ and η. When $\mathsf{K_s}$ (i.e. ν_{eq}) and η (i.e. ν_{c}) are constants, $\mathrm{Z}_{\alpha\gamma}(z)$ takes the simple form given by (47). It must be noted that following [26], we have temporarily and seemingly arbitrarily[5] assumed $\mathrm{Z}_{\alpha\gamma}(1) = 1$. Moreover, we also assume $v_z|_{z=0} \equiv v_z^{(1)}|_{z=0} = 0$ to ensure symmetric flow across the $z = 0$ plane[6] given the relation prescribed in (42).

$$\mathrm{Z}_{\alpha\gamma}(z) = \frac{(\mathsf{FN}^2 - \mathcal{B}_-)e^{\mathcal{B}_+ z} - (\mathsf{FN}^2 - \mathcal{B}_+)e^{\mathcal{B}_- z}}{(\mathsf{FN}^2 - \mathcal{B}_-)e^{\mathcal{B}_+} - (\mathsf{FN}^2 - \mathcal{B}_+)e^{\mathcal{B}_-}} \tag{47}$$

where,

$$\mathcal{B}_\pm = \frac{1}{2}[\mathsf{K_s} \pm (\mathsf{K_s}^2 + \eta^{-1}\mathsf{N}^2\lambda_{\alpha\gamma}^2)^{\frac{1}{2}}] \tag{48}$$

This is precisely the result achieved by van Eysden and Melatos [26] and Bennett et al. [7].

3.8 Temporal evolution

The temporal evolution of *Ekman pumping* is controlled by the boundary condition given by (42) [26, 2]. Taking the first-order derivative of (42) and using the results from the $O(\mathsf{E}^0)$ and $O(\mathsf{E}^{\frac{1}{2}})$ solutions, one arrives at the exponentially decaying time dependence[7] as follows,

$$\chi(r,\phi,z,t) = \sum_{\alpha=0}^{\infty}\sum_{\gamma=1}^{\infty} \mathsf{J}_\alpha(\lambda_{\alpha\gamma} r)\left[\frac{\mathrm{A}_{\alpha\gamma} - i\mathrm{B}_{\alpha\gamma}}{2} \times e^{i\alpha\phi} + \frac{\mathrm{A}_{\alpha\gamma} + i\mathrm{B}_{\alpha\gamma}}{2} e^{-i\alpha\phi}\right]\mathrm{Z}_{\alpha\gamma}(z) e^{-\omega_{\alpha\gamma} t} \tag{49}$$

where, momentarily assuming $\mathrm{Z}_{\alpha\gamma}(1)$ to be a physically nominal value that we will renew shortly,

$$\omega_{\alpha\gamma} = \frac{1}{4\mathsf{F}}\lambda_{\alpha\gamma}^2 \mathrm{Z}_{\alpha\gamma}(1)\left[\frac{\eta(1)}{\mathsf{FN}^2(1)}\frac{\partial \mathrm{Z}_{\alpha\gamma}}{\partial z}\bigg|_{z=1} + \left\{\frac{-\partial_z \eta|_{z=1}}{\mathsf{FN}^2(1)} - 1\right\}\mathrm{Z}_{\alpha\gamma}(1)\right]^{-1} \tag{50}$$

which for the simple case of $\mathsf{K_s}(z), \eta \rightarrow$ constant and $\mathrm{Z}_{\alpha\gamma}(1) = 1$, reduces to

$$\omega_{\alpha\gamma} = \frac{\lambda_{\alpha\gamma}^2\left[(\mathsf{FN}^2 - \mathcal{B}_-)e^{\mathcal{B}_+} - (\mathsf{FN}^2 - \mathcal{B}_+)e^{\mathcal{B}_-}\right]}{(4\mathsf{FK} + \lambda_{\alpha\gamma}^2)(e^{\mathcal{B}_+} - e^{\mathcal{B}_-})} \tag{51}$$

Now, given the explicit dependence of χ on time, we can integrate (49) over $t \in [t, \infty)$ and get

$$\frac{\delta p^{(0)}(r,\phi,z,t)}{\rho(z)} = \frac{\delta p^{(0)}_{t\rightarrow\infty}(r,\phi,z)}{\rho(z)} + \sum_{\alpha=0}^{\infty}\sum_{\gamma=1}^{\infty} \omega_{\alpha\gamma}^{-1} \times \mathsf{J}_\alpha(\lambda_{\alpha\gamma} r)[\mathrm{A}_{\alpha\gamma}\mathsf{Cos}(\alpha\phi) + \mathrm{B}_{\alpha\gamma}\mathsf{Sin}(\alpha\phi)] \times \mathrm{Z}_{\alpha\gamma}(z) e^{-\omega_{\alpha\gamma} t} \tag{52}$$

[5] While this may seem arbitrary, it is really not so; the function $\mathrm{Z}_{\alpha\gamma}(z)$ must be explicitly re-normalised to be in the range $[0, 1]$, since (41) dictates that χ - as a dimensionless variable - must be of the order $O(\mathsf{E}^0) \equiv 1$; it requires $\mathrm{Z}_{\alpha\gamma}(z)$ to be of the same order in magnitude.

[6] It can be easily deducted that the boundary condition on axial flow, $v_z|_{z=0} \equiv v_z^{(1)}|_{z=0} = 0$, is simply equivalent to specifying $\mathrm{Z}_{\alpha\gamma}(z)$ at $z = 0$ which is apparent from (39).

[7] Refer to section **A.1** in ***Appendix* A** for details

where, clearly the first term on the right-hand side is the constant of integration evaluated at $t \to \infty$ i.e. the steady-state pressure profile of the spun-up cylinder. The relation given by (52) essentially depicts the variation of pressure perturbation(s) to the first-order in magnitude as a function of time.

3.9 Initial and final conditions

We are now faced with one intrinsic degrees of freedom in our analysis (besides the *Bessel-Fourier coefficients*), which is the set of initial and final conditions at $t = 0$ i.e. immediately following the glitch, and $t \to \infty$ respectively. In principle, one can choose from an infinite set of possibilities. For example, ***a)*** one can assume a scenario where the modes continuously grow from an axisymmetric state in the post-glitch phase at $t = 0$ and then reach a steady non-axisymmetric state as $t \to \infty$, and remain in that state. This leads to emission of gravitational waves even at $t \to \infty$ on very large time-scales, and is somewhat unphysical. This also equates to the scenario of 'semi-rigidity', where the top and bottom faces of the cylinder rotate differentially at $t \to \infty$, potentially causing the crust to crack [26]. On the contrary, ***b)*** another alternative scenario is where the modes are instantaneously excited at $t = 0$ and decay eventually as $t \to \infty$, which is more physical in principle. This choice disallows for any residual non-axisymmetric motions in the bulk, ensures zero residual steady-state emission, and also incorporates the feature of rigidity between the two faces of the cylinder [7]. Both these possibilities are encoded in the choice of our assumed solutions at $t = 0$ and $t \to \infty$. However, the characteristics of modes as $t \to \infty$ (i.e. when *Ekman pumping* stops) is in fact coupled to their state at $t = 0$ by the relation (52), leaving us a free choice at either $t = 0$ or $t \to \infty$. Hence, we choose the more physical set of initial and final conditions where the modes originate arbitrarily and instantaneously at $t = 0$, and decay implicitly from some initial value $\delta\mathsf{P}_0$ to a symmetric steady-state $\delta\mathsf{P}_\infty = 0$ when $t \to \infty$ according to (52). Moreover, in presence of the term $\vec{v}_\mathsf{B}$ in (42), the equivalent steady state solution at $t \to \infty$ reaches an axisymmetric state with no angular dependence and only radial dependence [7], as opposed to the fully decayed state in absence of $\vec{v}_\mathsf{B}$. This axisymmetric state doesn't lead to any gravitational wave emission either, and allows us to continue ignoring the possible inclusion of $\vec{v}_\mathsf{B}$. Finally, under such a choice for a steady state at $t \to \infty$,

$$\delta\mathsf{P}_0 = \sum_{\alpha=0}^{\infty}\sum_{\gamma=1}^{\infty} \omega_{\alpha\gamma}^{-1}\mathsf{J}_\alpha(\lambda_{\alpha\gamma}r)[\mathrm{A}_{\alpha\gamma}\mathsf{Cos}(\alpha\phi) + \mathrm{B}_{\alpha\gamma}\times \mathsf{Sin}(\alpha\phi)]\mathrm{Z}_{\alpha\gamma}(z) = \sum_{\alpha=0}^{\infty} \mathrm{C}_\alpha r^\alpha(r^2-1)\mathsf{Cos}(\alpha\phi)\,\mathrm{Z}_{\alpha\gamma}(z) \tag{53}$$

where, wherever suitable from this point onward, we will abbreviate for simplicity of expression,

$$\delta\mathsf{P}_{t'} \equiv \frac{\delta p^{(0)}_{t\to t'}(r,\phi,z)}{\rho(z)}$$

C_α are the relative weights of modes excited at $t = 0$ and assumed to be equal to 1. Moreover, it must be noted that any assumed solution must be constrained by the boundary conditions on velocity-flow via (42), and be a solution to the Navier-Stokes equation by satisfying the relations in (17)-(19). Our assumed solution here guarantees the decay of all modes at $t \to \infty$, while it also ensures that the flow vanishes at the lateral surface at $r = \mathrm{L}$. We have assumed a trivial z-dependence as well as reduced dependence on ϕ for simplicity [26, 7], without potentially corrupting the generality of the solutions. The associated *Bessel-Fourier coefficients* $\mathrm{A}_{\alpha\gamma}$ and $\mathrm{B}_{\alpha\gamma}$ can now be calculated[8] as an implicit function of z:

$$\mathrm{A}_{\alpha\gamma} = \frac{2\omega_{\alpha\gamma}}{\pi \mathsf{J}^2_{\alpha+1}(\lambda_{\alpha\gamma})}\int_0^{2\pi}\mathrm{d}\phi\int_0^1\mathrm{d}z\int_0^1 r\,\mathrm{d}r\times \mathsf{J}_\alpha(\lambda_{\alpha\gamma}r)\,\mathsf{Cos}(\alpha\phi)\,[\delta\mathsf{P}_0 - \delta\mathsf{P}_\infty]\,\mathrm{Z}^{-1}_{\alpha\gamma}(z) = \frac{2\mathrm{C}_\alpha\,\omega_{\alpha\gamma}}{\mathsf{J}^2_{\alpha+1}(\lambda_{\alpha\gamma})}\int_0^1 \mathrm{d}r\, r^{\alpha+1}(r^2-1)\mathsf{J}_\alpha(\lambda_{\alpha\gamma}r) \tag{54}$$

and,

$$\mathrm{B}_{\alpha\gamma} = \frac{2\omega_{\alpha\gamma}}{\pi \mathsf{J}^2_{\alpha+1}(\lambda_{\alpha\gamma})}\int_0^{2\pi}\mathrm{d}\phi\int_0^1\mathrm{d}z\int_0^1 r\,\mathrm{d}r\times \mathsf{J}_\alpha(\lambda_{\alpha\gamma}r)\,\mathsf{Sin}(\alpha\phi)\,[\delta\mathsf{P}_0 - \delta\mathsf{P}_\infty]\,\mathrm{Z}^{-1}_{\alpha\gamma}(z) = 0 \tag{55}$$

In principle, the *Bessel-Fourier coefficients* may not be constants. In fact, they might well be functions of ϕ and z depending on the chosen initial condition in (53). However, since we chose trivial dependence on ϕ and z in our assumed initial condition in (53), this leads to $\mathrm{A}_{\alpha\gamma}$ and $\mathrm{B}_{\alpha\gamma}$ being constants. The first few values of $\mathrm{A}_{\alpha\gamma}$ are: $\mathrm{A}_{11} = -0.706\,\omega_{11}$, $\mathrm{A}_{21} = -0.521\,\omega_{21}$, $\mathrm{A}_{12} = 0.154\,\omega_{12}$, and $\mathrm{A}_{22} = 0.148\,\omega_{22}$.

3.10 Final solutions

We now have all ingredients to restore the dimensions and calculate the final *velocity*, *density*, and *pressure* fields in the inertial rest frame instead of the rotating Lagrangian frame. The result for density profile in the inertial frame is then given by

$$\rho(r,\phi,z,t) = \rho_0\rho_e(z/\mathrm{L}) + \rho_0\frac{(\delta\Omega)\Omega\mathrm{L}}{g}\times \sum_{\alpha=0}^{\infty}\sum_{\gamma=1}^{\infty}\omega^{-1}_{\alpha\gamma}\mathrm{C}_\alpha\mathrm{A}_{\alpha\gamma}\mathsf{J}_\alpha\left(\frac{\lambda_{\alpha\gamma}r}{\mathrm{L}}\right)\mathsf{Cos}[\alpha(\phi-\Omega t)]\times \partial_z[-\mathrm{L}\,\mathrm{Z}_{\alpha\gamma}(z/\mathrm{L})\rho_e(z/\mathrm{L})]e^{-\mathsf{E}^{\frac{1}{2}}\omega_{\alpha\gamma}\Omega t} \tag{56}$$

[8] Refer to section **A.2** in ***Appendix* A** for details

whereas, from (34),

$$\delta\rho^{(0)}_{t\to 0}(r,\phi,z) = -\partial_z[\rho(z)\delta P_0] = -\left[\sum_{\alpha=0}^{\infty} C_\alpha\, r^\alpha (r^2-1)\mathrm{Cos}(\alpha\phi)\right]\frac{\partial[\rho(z)]}{\partial z} \quad (57)$$

while $\delta v_r^{(0)}(r,\phi,z,t\to 0)$ and $\delta v_\phi^{(0)}(r,\phi,z,t\to 0)$ can be similarly calculated from (31) and (32) respectively. Moreover, we can also calculate the pressure profile, and the velocity field characteristics up to the order $O(E^{\frac{1}{2}})$ as given below using (31)-(33) and (39),

$$p(r,\phi,z,t) = \rho_0 g L\, p_e(z/L) + \left[\rho_0(\delta\Omega)\Omega L^2 \sum_{\alpha=0}^{\infty}\sum_{\gamma=1}^{\infty} \omega_{\alpha\gamma}^{-1} C_\alpha A_{\alpha\gamma} J_\alpha\left(\frac{\lambda_{\alpha\gamma} r}{L}\right) Z_{\alpha\gamma}(z/L)\times \mathrm{Cos}[\alpha(\phi-\Omega t)]\,\rho_e(z/L) e^{-E^{\frac{1}{2}}\omega_{\alpha\gamma}\Omega t}\right] \quad (58)$$

$$\delta v_r \equiv \delta v_r^{(0)}(r,\phi,z,t) = \frac{1}{2}(\delta\Omega)L^2 \sum_{\alpha=0}^{\infty}\sum_{\gamma=1}^{\infty} \frac{\alpha}{r}\omega_{\alpha\gamma}^{-1} C_\alpha \times A_{\alpha\gamma} J_\alpha\left(\frac{\lambda_{\alpha\gamma} r}{L}\right)\mathrm{Cos}[\alpha(\phi-\Omega t)]\, Z_{\alpha\gamma}(z/L) e^{-E^{\frac{1}{2}}\omega_{\alpha\gamma}\Omega t} \quad (59)$$

$$\delta v_\phi \equiv \delta v_\phi^{(0)}(r,\phi,z,t) = \Omega r + \frac{1}{2}(\delta\Omega)L \sum_{\alpha=0}^{\infty}\sum_{\gamma=1}^{\infty} \omega_{\alpha\gamma}^{-1}\times C_\alpha A_{\alpha\gamma}\lambda_{\alpha\gamma}\,\partial_r\left[L\, J_\alpha\left(\frac{\lambda_{\alpha\gamma} r}{L}\right)\right]\mathrm{Cos}[\alpha(\phi-\Omega t)]\times Z_{\alpha\gamma}(z/L) e^{-E^{\frac{1}{2}}\omega_{\alpha\gamma}\Omega t} \quad (60)$$

and[9],

$$\delta v_z \equiv v_z^{(1)}(r,\phi,z,t) = \frac{1}{FN^2(z)}\frac{\partial\chi}{\partial z} - \chi \equiv O(E^{\frac{1}{2}}) \quad \text{(in dimensionless units)}; \quad (61)$$

4 Gravitational wave emission

In this section, we will calculate the gravitational wave signal emission from mass-quadrupole and current-quadrupole moments of the non-axisymmetric flow characteristics derived in section 3.

4.1 Gravitational wave emission via mass-quadrupole

The density, pressure and velocity fields calculated in the previous section may lead to gravitational wave emission if the corresponding distribution and flow characteristics are non-axisymmetric in nature, at the very least. In fact, any such non-vanishing non-axisymmetry could lead to a non-zero mass-quadrupole moment – with at least second-order non-vanishing time-derivative – at the lowest order leading to emission of gravitational wave signal. We will not delve into the mathematical details of the emission here and arrive at the following result straightaway[10] for the + and × polarizations for a *polar observer* (for an observer located at a distance d_{source} along the rotation axis of the neutron star),

$$h_+^{M^P}(t) = h_o^M \sum_{\gamma=1}^{\infty}\kappa_{2\gamma}\Big[-4\omega_{2\gamma} E^{\frac{1}{2}}\,\mathrm{Sin}(2\Omega t) + (4 - E\omega_{2\gamma}^2)\mathrm{Cos}(2\Omega t)\Big] e^{-E^{\frac{1}{2}}\omega_{2\gamma}\Omega t} \quad (62)$$

$$h_\times^{M^P}(t) = h_o^M \sum_{\gamma=1}^{\infty}\kappa_{2\gamma}\Big[-4\omega_{2\gamma} E^{\frac{1}{2}}\,\mathrm{Cos}(2\Omega t) - (4 - E\omega_{2\gamma}^2)\,\mathrm{Sin}(2\Omega t)\Big] e^{-E^{\frac{1}{2}}\omega_{2\gamma}\Omega t} \quad (63)$$

where the full expression of $\kappa_{\alpha\gamma}$ is too lengthy to quote here and is given in section **A.5** in ***Appendix* A**. The characteristic dimensionless strain magnitude h_o, and $t_{\alpha\gamma}$ – the relaxation time-scale for the $\{\alpha,\gamma\}$th mode – are given by

$$h_o^M = \pi\rho_o\Omega^4 L^6 \epsilon\frac{G}{c^4 d_{\mathrm{source}} g} \quad (64)$$

$$t_{\alpha\gamma} = E^{-\frac{1}{2}}\Omega^{-1}\omega_{\alpha\gamma}^{-1} \quad (65)$$

where, $\kappa_{2\gamma}$ and h_o^M are both constant quantities. We may transform the expressions (62)-(63) for time-series amplitudes to the more useful Fourier space for a polar observer as follows[11],

$$|h_+^{M^P}(\omega)|^2 = h_o^{M^2}\sum_{\gamma=1}^{\infty}|\kappa_{2\gamma}|^2\Big\{\Big[t_{2\gamma}^{-2}(4+t_{2\gamma}^{-2}\Omega^{-2})^2 + \omega^2(4-t_{2\gamma}^{-2}\Omega^{-2})^2\Big]\Big[(4\Omega^2+t_{2\gamma}^{-2}-\omega^2)^2+(2\omega t_{2\gamma}^{-1})^2\Big]^{-1}\Big\} \quad (66)$$

$$|h_\times^{M^P}(\omega)|^2 = h_o^{M^2}\sum_{\gamma=1}^{\infty}|\kappa_{2\gamma}|^2\Big\{\Big[4\Omega^2(4+t_{2\gamma}^{-2}\Omega^{-2})^2 + 16\omega^2 t_{2\gamma}^{-2}\Omega^{-2}\Big]\Big[(4\Omega^2+t_{2\gamma}^{-2}-\omega^2)^2+(2\omega t_{2\gamma}^{-1})^2\Big]^{-1}\Big\} \quad (67)$$

[9] We have left the expression unmentioned in explicit form since the only contribution comes from $O(E^{\frac{1}{2}})$, which is an order lower than the magnitudes we want to explore.

[10] Refer to section **A.3** in ***Appendix* A** for details of calculation.

[11] δ_D is the *Kronecker Delta function* with units of Hz^{-1}.

Clearly, $|h_+^{\mathrm{M^P}}(\omega)|$ and $|h_\times^{\mathrm{M^P}}(\omega)|$ exhibit resonance at $\omega_{\mathrm{R}}^2 = 4\Omega^2 + t_{2\gamma}^{-2}$. Now, a similar analysis can be made for an *equatorial observer*, and the corresponding results are given by

$$h_+^{\mathrm{M^E}}(t) = \frac{1}{2}h_{\mathrm{o}}^{\mathrm{M}}\sum_{\gamma=1}^{\infty}\kappa_{2\gamma}\Big[-4\omega_{2\gamma}\mathsf{E}^{\frac{1}{2}}\,\mathsf{Sin}(2\Omega t)+ (4-\mathsf{E}\omega_{2\gamma}^2)\mathsf{Cos}(2\Omega t)\Big]e^{-\mathsf{E}^{\frac{1}{2}}\omega_{2\gamma}\Omega t} \tag{68}$$

$$h_\times^{\mathrm{M^E}}(t) = 2h_{\mathrm{o}}^{\mathrm{M}}\sum_{\gamma=1}^{\infty}\kappa_{1\gamma}\Big[2\omega_{1\gamma}\mathsf{E}^{\frac{1}{2}}\,\mathsf{Cos}(\Omega t)+ (1-\mathsf{E}\omega_{1\gamma}^2)\,\mathsf{Sin}(\Omega t)\Big]e^{-\mathsf{E}^{\frac{1}{2}}\omega_{1\gamma}\Omega t} \tag{69}$$

It is important to note the change of oscillating frequency for the $\times$ polarization from 2Ω in case of a *polar observer* to Ω in case of an *equatorial observer*. Further, additional 1γ modes, as seen by *equatorial observer*, appear besides the 2γ modes in the emission spectrum. In fourier space for an equatorial observer, we have:

$$|h_+^{\mathrm{M^E}}(\omega)|^2 = \frac{1}{4}h_{\mathrm{o}}^{\mathrm{M}^2}\sum_{\gamma=1}^{\infty}|\kappa_{2\gamma}|^2\Big\{\Big[t_{2\gamma}^{-2}(4+t_{2\gamma}^{-2}\Omega^{-2})^2 + \omega^2(4-t_{2\gamma}^{-2}\Omega^{-2})^2\Big]\Big[(4\Omega^2+t_{2\gamma}^{-2}-\omega^2)^2+(2\omega t_{2\gamma}^{-1})^2\Big]^{-1}\Big\} \tag{70}$$

$$|h_\times^{\mathrm{M^E}}(\omega)|^2 = 4h_{\mathrm{o}}^{\mathrm{M}^2}\sum_{\gamma=1}^{\infty}|\kappa_{1\gamma}|^2\Big\{\Big[\Omega^2(1+t_{1\gamma}^{-2}\Omega^{-2})^2 + 4\omega^2 t_{1\gamma}^{-2}\Omega^{-2}\Big]\Big[(\Omega^2+t_{1\gamma}^{-2}-\omega^2)^2+(2\omega t_{1\gamma}^{-1})^2\Big]^{-1}\Big\} \tag{71}$$

In this case, $|h_+^{\mathrm{M^E}}(\omega)|$ exhibits resonance at $\omega_{\mathrm{R}}^2 = 4\Omega^2 + t_{2\gamma}^{-2}$, while $|h_\times^{\mathrm{M^E}}(\omega)|$ exhibits resonance at $\omega_{\mathrm{R}}^2 = \Omega^2 + t_{1\gamma}^{-2}$. It is worth noting that the factors $\kappa_{1\gamma}$, $\kappa_{2\gamma}$ decrease in magnitude with increasing index γ, and we can truncate the above expressions at leading order $\gamma = 1$. The maximum effective magnitude of the emitted gravitational waves for both polarizations at a given frequency ω then depends strongly on the characteristic magnitude $h_{\mathrm{o}}^{\mathrm{M}}$ and its amplification by the frequency terms in the fourier transforms. There also exists a weak dependency on the pre-factors $|\kappa_{1\gamma}|$ and $|\kappa_{2\gamma}|$[12]. Below in figure 2 and figure 3, we plot the frequency characteristics[13] of the emitted signal strengths for $|h_+^{\mathrm{M^P}}(\omega)|$, $|h_\times^{\mathrm{M^P}}(\omega)|$, $|h_+^{\mathrm{M^E}}(\omega)|$ and $|h_\times^{\mathrm{M^E}}(\omega)|$.

4.2 Gravitational wave emission via current-quadrupole

Gravitational wave emission from mass-quadrupole occurs when the associated oscillating mass-quadrupole moment – time-varying at least up to second-order – excites gravitational waves. However, it is also possible to include the current-quadrupole contribution from the effect of time-variation in the intrinsic mass-distribution (also referred to as *mass-currents*) of the bulk matter [24, 7]. This effect is a subset of the *gravitomagnetic effects*, the electromagnetic equivalent in gravitation: similar to the case of electromagnetism where electric charges and current multipoles emit electromagnetic radiation, time-varying mass-current multipoles can also emit gravitational wave radiation, besides the emission from mass-quadrupole moment. We straightaway produce the expressions for the + and $\times$ polarization following Thorne [24], Melatos and Peralta [17] and Bennett et al. [7] for a *polar observer* as follows[14],

$$h_+^{\mathrm{C^P}}(t) = h_{\mathrm{o}}^{\mathrm{C}}\sum_{\gamma=1}^{\infty}\mathsf{V}_{2\gamma}\Big[-4t_{2\gamma}^{-1}\Omega^{-1}\mathsf{Cos}(2\Omega t)- (4-t_{2\gamma}^{-2}\Omega^{-2})\mathsf{Sin}(2\Omega t)\Big]e^{-t_{2\gamma}^{-1}t} \tag{72}$$

$$h_\times^{\mathrm{C^P}}(t) = h_{\mathrm{o}}^{\mathrm{C}}\sum_{\gamma=1}^{\infty}\mathsf{V}_{2\gamma}\Big[-4t_{2\gamma}^{-1}\Omega^{-1}\mathsf{Sin}(2\Omega t)+ (4-t_{2\gamma}^{-2}\Omega^{-2})\mathsf{Cos}(2\Omega t)\Big]e^{-t_{2\gamma}^{-1}t} \tag{73}$$

and, for an *equatorial observer* as given below by

$$h_+^{\mathrm{C^E}}(t) = 2h_{\mathrm{o}}^{\mathrm{C}}\sum_{\gamma=1}^{\infty}\mathsf{V}_{1\gamma}\Big[2t_{1\gamma}^{-1}\Omega^{-1}\mathsf{Cos}(\Omega t)+ (1-t_{1\gamma}^{-2}\Omega^{-2})\mathsf{Sin}(\Omega t)\Big]e^{-t_{1\gamma}^{-1}t} \tag{74}$$

$$h_\times^{\mathrm{C^E}}(t) = \frac{1}{2}h_{\mathrm{o}}^{\mathrm{C}}\sum_{\gamma=1}^{\infty}\mathsf{V}_{2\gamma}\Big[-4t_{2\gamma}^{-1}\Omega^{-1}\mathsf{Sin}(2\Omega t)+ (4-t_{2\gamma}^{-2}\Omega^{-2})\mathsf{Cos}(2\Omega t)\Big]e^{-t_{2\gamma}^{-1}t} \tag{75}$$

where,

$$h_{\mathrm{o}}^{\mathrm{C}} = 2\pi\rho_{\mathrm{o}}\Omega^3\mathrm{L}^6\,\epsilon\frac{\mathrm{G}}{3c^5 d_{\mathsf{source}}} \tag{76}$$

We have again restricted ourselves to the leading-order quadrupole term $l = 2$ of the mass-current multipole expansion. Once more, we may write the above expressions for *polar* and *equatorial* observers in the fourier space. In case of a *polar observer*, this reduces to

[12] The 'weak' dependency in this case refers to the fact that $|\kappa_{1\gamma}|$ and $|\kappa_{2\gamma}|$ are not as sensitive to variations in $\mathsf{K_s}$ or N^2, as we will see in later sections.

[13] In order to show the frequency characteristic, we abbreviate the remaining factors for simplicity such that $\left[\frac{|h_\mp^{\mathcal{L}^{\mathsf{Y}}}(\omega)|}{h_{\mathrm{o}}^{\mathcal{L}}|\kappa_{\alpha\gamma}|}\right]^2 \equiv \mathsf{G}_{\mp|\alpha\gamma}^{\mathcal{L}^{\mathsf{Y}}}$.

[14] Refer to section **A.4** in ***Appendix A*** for more details of the calculation and expressions for the involved pre-factors $\mathsf{V}_{1\gamma}$ and $\mathsf{V}_{2\gamma}$.

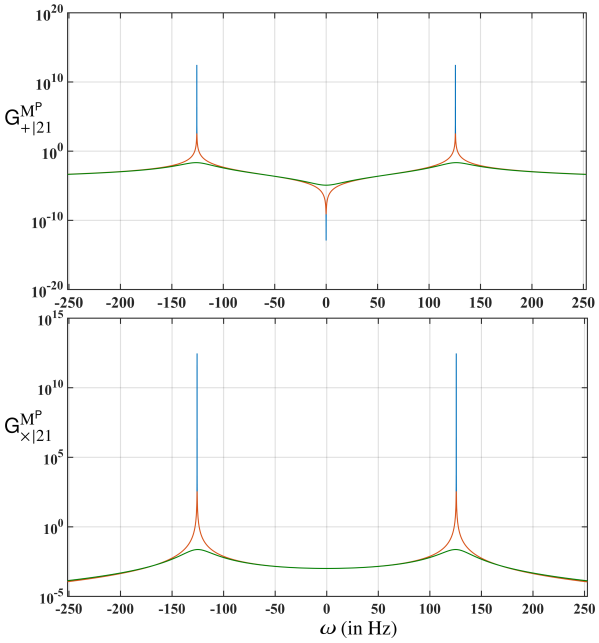

Figure 2: Frequency characteristics of emitted signals for *polar observer*: 3 different set of data are plotted above for a rotational frequency of 10 Hz and $\partial_z\eta \to 10^{-11}$. The respective color coded time-scales are 9.837 d, 1.084×10^{-4} d and 8.518×10^{-7} d. The corresponding resonant frequencies are $\pm125.66370614359 17$, ±125.6637513749575 and ±126.3961088409387 Hz. Note that the values of time-scales are calculated for specifically chosen independent system parameters v_c, $\partial_z\eta$, v_{eq}, K, and F, in order to cover a large range of time-scales.

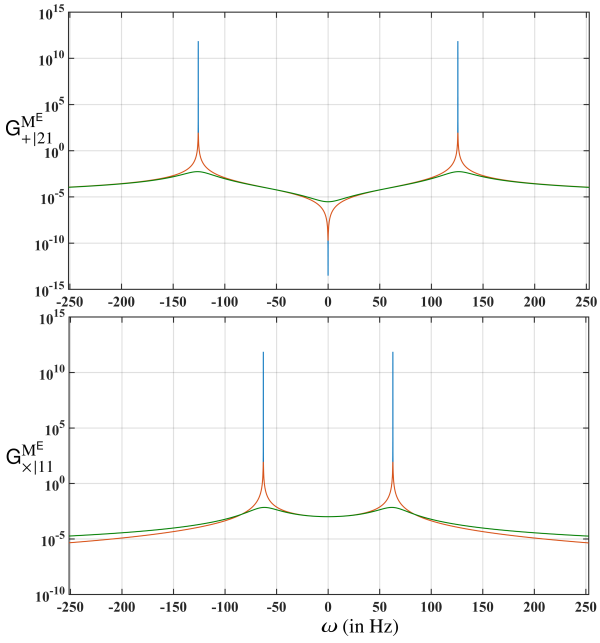

Figure 3: Frequency characteristics of emitted signals for *equatorial observer*: 3 different set of data are plotted above at a rotational frequency of 10 Hz and $\partial_z\eta \to 10^{-11}$. The respective color coded time-scales are 9.837 d, 1.084×10^{-4} d and 8.518×10^{-7} d. Moreover, the corresponding resonant frequencies for $\times$ polarization are ±62.831853071795848, ±62.831875687478750, ±63.198054420469347 Hz, whereas the resonant frequencies for the + polarization remain exactly the same as they were previously for the case of a *polar observer*.

$$|h^{C^P}_{+}(\omega)|^2 = h^{C^2}_{o}\sum_{\gamma=1}^{\infty}|V_{2\gamma}|^2\Big\{\Big[4\Omega^2(4+t_{2\gamma}^{-2}\Omega^{-2})^2 + 16\omega^2 t_{2\gamma}^{-2}\Omega^{-2}\Big]\Big[(4\Omega^2+t_{2\gamma}^{-2}-\omega^2)^2+(2\omega t_{2\gamma}^{-1})^2\Big]^{-1}\Big\} \tag{75}$$

$$|h^{C^P}_{\times}(\omega)|^2 = h^{C^2}_{o}\sum_{\gamma=1}^{\infty}|V_{2\gamma}|^2\Big\{\Big[t_{2\gamma}^{-2}(4+t_{2\gamma}^{-2}\Omega^{-2})^2 + \omega^2(4-t_{2\gamma}^{-2}\Omega^{-2})^2\Big]\Big[(4\Omega^2+t_{2\gamma}^{-2}-\omega^2)^2+(2\omega t_{2\gamma}^{-1})^2\Big]^{-1}\Big\} \tag{76}$$

It must be noted that the resonant frequencies for current-quadrupole contribution from $|h^{M^P}_{+}(\omega)|$ and $|h^{M^P}_{\times}(\omega)|$ are the same as they were for mass-quadrupole contribution. Further, for the case of *equatorial observers*,

$$|h^{C^E}_{+}(\omega)|^2 = 4h^{C^2}_{o}\sum_{\gamma=1}^{\infty}|V_{1\gamma}|^2\Big\{\Big[\Omega^2(1+t_{1\gamma}^{-2}\Omega^{-2})^2 + 4\omega^2 t_{1\gamma}^{-2}\Omega^{-2}\Big]\Big[(\Omega^2+t_{1\gamma}^{-2}-\omega^2)^2+(2\omega t_{1\gamma}^{-1})^2\Big]^{-1}\Big\} \tag{77}$$

$$|h^{C^E}_{\times}(\omega)|^2 = \frac{1}{4}h^{C^2}_{o}\sum_{\gamma=1}^{\infty}|V_{2\gamma}|^2\Big\{\Big[t_{2\gamma}^{-2}(4+t_{2\gamma}^{-2}\Omega^{-2})^2 + \omega^2(4-t_{2\gamma}^{-2}\Omega^{-2})^2\Big]\Big[(4\Omega^2+t_{2\gamma}^{-2}-\omega^2)^2+(2\omega t_{2\gamma}^{-1})^2\Big]^{-1}\Big\} \tag{78}$$

One can see that the emitted signals from the mass-quadrupole and the current-quadrupole are similar in nature in terms of the resonant frequencies and the general behavior of the frequency responses[15]. However, there is a rather notable switch in the + and × polarizations. Additionally, $V_{1\gamma}$ and $V_{2\gamma}$ pre-factors now appear instead of $\kappa_{1\gamma}$ and $\kappa_{2\gamma}$, as well as the different characteristic amplitudes. Lastly, the frequency characteristics for $|h^{C^P}_{+}(\omega)|$, $|h^{C^P}_{\times}(\omega)|$, $|h^{C^E}_{\times}(\omega)|$ and $|h^{C^E}_{+}(\omega)|$ follow the same shapes as shown previously in figure 2 and figure 3.

4.3 A verdict on parameter space

It is evident from the general expressions of $\kappa_{\alpha\gamma}$ (in section **A.5** in ***Appendix A***) and $V_{\alpha\gamma}$ (in section **A.4** in ***Appendix A***) that their calculations can be cumbersome to

[15] The characteristic amplitudes for mass and current quadrupole are related by $\frac{|h^{C}_{o}|}{|h^{M}_{o}|} = \frac{2g}{3\Omega c}$.

perform unless one could make some simplifying assumptions. Ideally, one would like to explore the range of parameter space where the first derivative of η – i.e. $\partial_z\eta$ in (51) and $\partial_z \mathsf{K_s}$ are constants, and follow

$$\begin{aligned} |\partial_z\eta| \ll \mathsf{F}\mathsf{N}^2 \ll \eta < 1 \quad &\text{for} \quad \forall\ z \in (0,1] \\ |\partial_z \mathsf{K_s}| \ll |\mathsf{K_s}| \quad &\text{for} \quad \forall\ z \in (0,1] \end{aligned} \tag{79}$$

Such a choice of a regime leaves the calculations analytically feasible. At the same time, it is possible to relax the aforementioned assumptions somewhat as we will explore now. In the meantime, we want to avoid having to explicitly and completely write down model forms of v_c and v_eq with respect to z-coordinate. One can do this to the first-order by studying to the regime where v_c is linear in z and takes the form,

$$v_\mathrm{c}(z) = v_\mathrm{c}^\mathrm{o} + z \times \partial_z v_\mathrm{c}, \tag{80}$$

such that, at the same time, N^2 is also a constant. These assumptions leave v_eq implicitly varying in z according to (28). It must be noted that this doesn't imply constancy of η; in fact, it yields that $\partial_z\eta \to 2v_\mathrm{c}(z)\partial_z v_\mathrm{c}$, and $\partial_z^2\eta \to 2(\partial_z v_\mathrm{c})^2$. Lastly, we are left with N^2, v_c^o and $\partial_z v_\mathrm{c}$ as free parameters to base our analysis on; $\mathsf{K_s}$ (or, v_eq) in this case becomes a dependent parameter varying in z according to (28). We will, thus, only restrict ourselves to the domain where

$$|\partial_z v_\mathrm{c}| \ll v_\mathrm{c}^\mathrm{o} < 1 \implies |\partial_z \mathsf{K_s}| \ll |\mathsf{K_s}|, \partial_z\eta \to 2v_\mathrm{c}^\mathrm{o}\partial_z v_\mathrm{c} \tag{81}$$

Under such assumptions, the calculations for the factors $\kappa_{\alpha\gamma}$ and $\mathsf{V}_{\alpha\gamma}$ become analytically derivable[16] when compared with analysis for explicit models of v_c and v_eq; it occurs simply because $\partial_z\eta$ is now effectively invariant in z according to (81). Furthermore, these simplifying assumptions are also helpful in avoiding the numerical errors which dominate significantly in the calculations of $\kappa_{\alpha\gamma}$ and $\mathsf{V}_{\alpha\gamma}$ at lower ranges of v_c^o – catalysed by large corresponding magnitudes of $\mathsf{K_s}$ below roughly $0.07c$. This effect is shown in detail in section **A.6** in ***Appendix* A** where we have compared numerical and analytically approximated results for $\kappa_{\alpha\gamma}$ and $\mathsf{V}_{\alpha\gamma}$. In nutshell, it is clear that the analytic approximation in (81) is indeed very useful on more than one front. The complete reduced expressions for $\kappa_{\alpha\gamma}$ and $\mathsf{V}_{\alpha\gamma}$ are given in section **A.5** in ***Appendix* A**.

It must be noted that such a limiting assumption of constancy of $\partial_z\eta$ isn't applied while calculating $\omega_{\alpha\gamma}$ and the corresponding time-scales $t_{\alpha\gamma}$, via (50). However, the time-scales $t_{\alpha\gamma}$ are not prone to the errors from numerical computations such as $\kappa_{\alpha\gamma}$ and $\mathsf{V}_{\alpha\gamma}$, and it remains straightforward to compute them numerically and accurately. If one wishes to use the assumptions set by (81), the approximated expression for the time-scales is given in section **A.5** in ***Appendix* A** [see (A.5.11)].

5 Time-scales of emitted signals and corresponding amplitudes

In this section, we explore the decay time-scales of the emitted signals. It can be seen from the expressions in (62)-(69) for the mass-quadrupole contribution, and (72)-(75) for the current-quadrupole contribution that the decay time-scale $t_{\alpha\gamma}$ for a given α, γ mode [as defined previously in (64)] is given by,

$$t_{\alpha\gamma} = \mathsf{E}^{-\frac{1}{2}}\Omega^{-1}\omega_{\alpha\gamma}^{-1} \tag{82}$$

The emitted gravitational wave signal strength at a given frequency ω depends intrinsically on the time-scale; this is apparent in the expressions in (62)-(78). We now have 3 independent parameters to vary: $v^\mathrm{o}\mathrm{c}$, $\partial_z v_\mathrm{c}$ and N^2, under the analytic approximations introduced within the previous section in (81). In figure 4, we plot the characteristics for the involved time-scales t_{11} and t_{21} [given that (81) holds], and the corresponding gravitational wave amplitudes for mass-quadrupole and current-quadrupole contributions at resonant frequencies i.e. $\omega = \omega_\mathrm{R}$ (denoted by subscript **R**). Note that resonant frequencies ω_R are also a function of $t_{\alpha\gamma}$, as shown in section 4.1. This corresponds to the effect where $|h_\times^{\mathsf{M}^\mathsf{E}}|$, $|h_+^{\mathsf{C}^\mathsf{E}}|$ emit at different resonant frequencies and different time-scales than $|h_\times^{\mathsf{M}^\mathsf{P}}|$, $|h_+^{\mathsf{M}^\mathsf{P}}|$, $|h_+^{\mathsf{M}^\mathsf{E}}|$, $|h_\times^{\mathsf{C}^\mathsf{P}}|$, $|h_+^{\mathsf{C}^\mathsf{P}}|$ and $|h_\times^{\mathsf{C}^\mathsf{E}}|$, as shown in figure 4.

Note that the case of $\partial_z v_\mathrm{c} < 0$ in figure 4 (rightmost panels) might seem interesting. The singular out-liar in the plots for $\partial_z v_\mathrm{c} = -10^{-4}$ is an artifact of low resolution in parameters space. In figure 5, we show the characteristics in the vicinity of the out-liar for clarity.

5.1 Growing modes

It is worth noting in the plots in figure 4 that for $\partial_z v_\mathrm{c} < 0$, it is possible to have *growing modes*. The *growing modes* refer to the cases where perturbations become unstable and start to experience monotonic growth instead of a damped relaxation. Without going into much detail, this effect can be reasoned with. In the case when $\partial_z v_\mathrm{c} = 0$, growing modes arise only when the classical *Brunt-Väisälä frequency* N_c^2[17] (as employed in [26, 7]) becomes negative. This happens when the constant adiabatic sound speed becomes less than the constant equilibrium sound speeds i.e. $v_\mathrm{c} < v_\mathrm{eq}$. However, this condition is a necessary one although not sufficient. In our case, where adiabatic and equilibrium sound speeds are allowed to vary in z-direction, similar effect may occur when $\partial_z v_\mathrm{c} < 0$ (or, $\partial_z\eta < 0$) such that $\mathsf{FN}^2 + \partial_z\eta < 0$.

[16] see section **A.5** in ***Appendix* A** for details and full expressions of $\kappa_{\alpha\gamma}$ and $\mathsf{V}_{\alpha\gamma}$.

[17] The classical *Brunt-Väisälä frequency* is given when adiabatic as well as the equilibrium sound speeds v_c and v_eq respectively are constants, by, $\mathsf{N}_\mathrm{c}^2 = g\mathsf{L}\mathsf{F}^{-1}(v_\mathrm{eq}^{-2} - v_\mathrm{c}^{-2})$

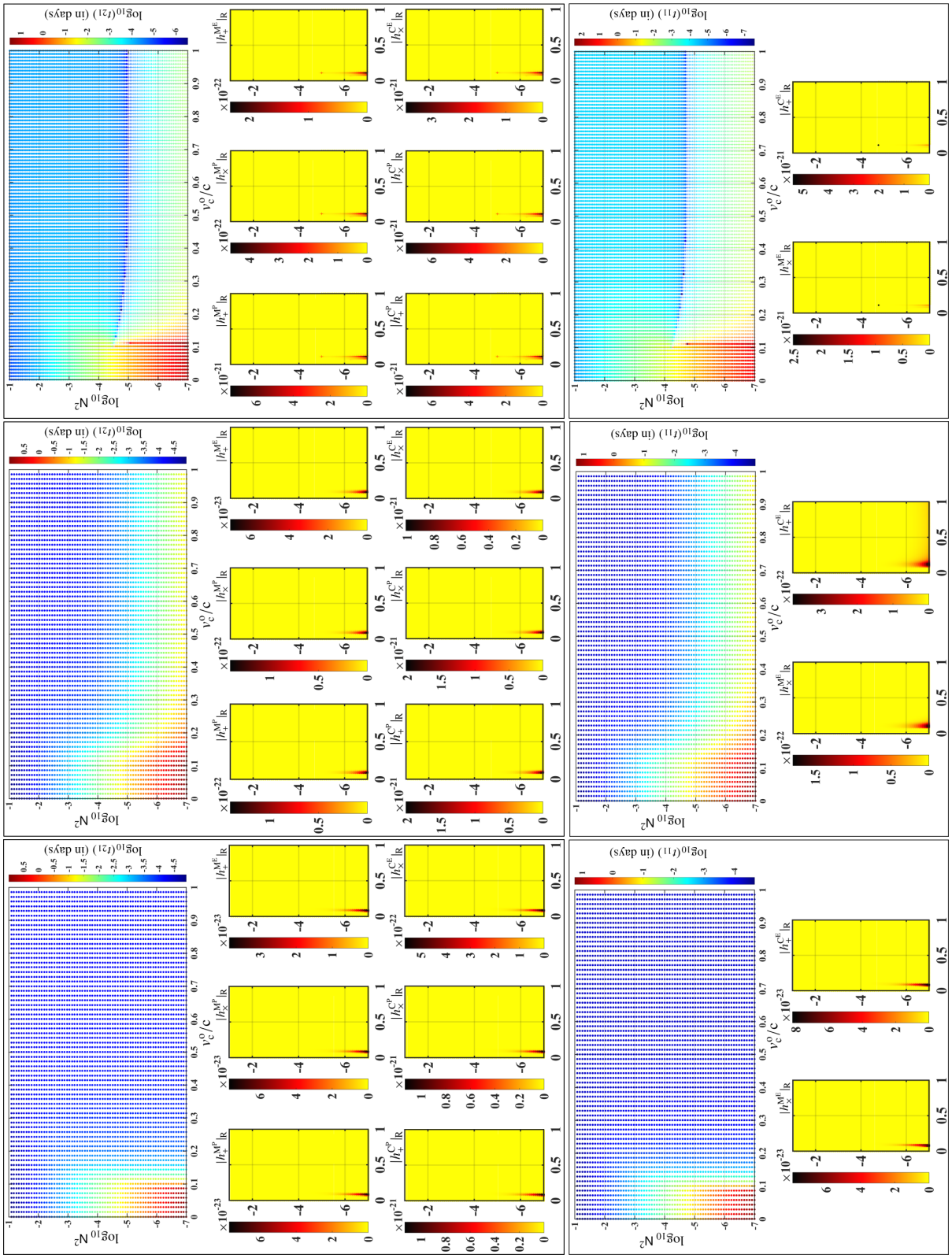

Figure 4: Emitted gravitational wave strain (*turn page sideways*): The top panel represents the time-scales for the t_{21} mode and the corresponding gravitational wave strain magnitudes for 3 sets of values for $\partial_{\mathcal{Y}} v_c$ at $0c$, $10^{-3}c$, $-10^{-4}c$ (left to right/bottom to top) respectively. The bottom panel shows the t_{11} modes, and corresponding gravitational wave strain magnitudes. The parameters are set to: $f = 100\,\mathrm{Hz}$, $\mathsf{E} = 10^{-7}$, $\epsilon = 10^{-4}$, $d_{\mathsf{source}} = 1.0\,\mathrm{kpc}$, $\mathrm{L} = 10^{4}\mathrm{m}$, $g = 10^{12}\mathrm{m/sec^2}$, $\rho_o = 10^{17}\mathrm{Kg/m^3}$. All positive time-scales as well as the corresponding emitted strains are marked by $\bullet$, while the negative time-scales and corresponding strains are marked by $+$.

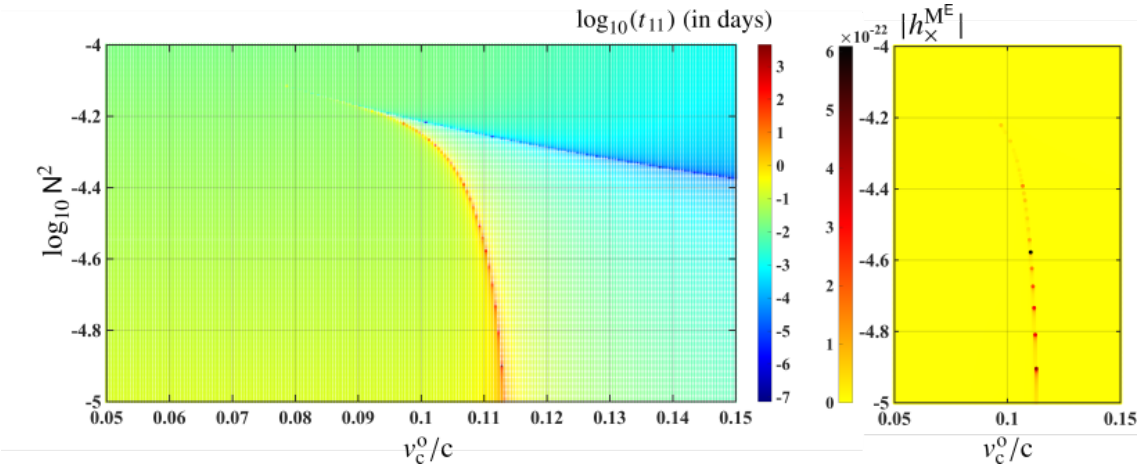

Figure 5: Out-liar zoomed in: The characteristics of the parameter space in the vicinity of the singular out-liar in figure 4 for the case of $\partial_z v_c = -10^{-4}$ (rightmost panels in figure 4) are shown in higher resolution. All positive time-scales as well as corresponding emitted strains are marked by •, while the negative time-scales and corresponding strains are marked by +.

One must carefully note that this again is not a sufficient condition although a necessary one. To step into a little more detail, $\mathsf{F}\mathsf{N}^2 + \partial_z \eta < 0$ may lead to $\partial_z[\mathrm{Z}_{\alpha\gamma}]|_{z=1}$ becoming negative in (50) and thus potentially causing growing modes. One such example is simulated in figure 6 showing the aforementioned affect.

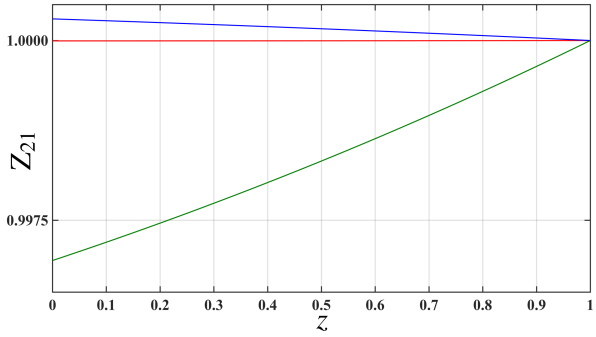

Figure 6: $\mathrm{Z}_{\alpha\gamma}$ characteristics: 3 different set of data are plotted for the t_{21} mode at a rotational frequency of 100 Hz, $\mathsf{N}^2 = 10^{-6}$, $v_c^o = 0.8c$, and for a set of values of $\partial_z v_c$; these respective color-coded set of values are given as $-10^{-4}c$, $10^{-3}c$, and 0. Note that the slope of Z_{21} tends to a negative value (especially $\partial_z[\mathrm{Z}_{21}]|_{z=1} < 0$) when $\partial_z v_c < 0$. In turn, the corresponding color-coded time-scales are calculated to be -5.9×10^{-4} d, 6.6×10^{-3} d and 6.4×10^{-5} d. This also reflects the sensitivity of time-scales to $\partial_z \eta$ or, $\partial_z v_c$.

The existence of such an affect can be debated, although the explanation is quite straightforward, at least physically. Growing modes may occur in cases where the chosen set of adiabatic and equilibrium sound speeds is such that the system appears to gain energy in time despite being in an isolated state. In our system, this is merely an analytic shortcoming which arises from not having an explicit relation for energy exchange (or, energy conservation) between the neutron star as a system and its surroundings. This affect is clear when the classical *Brunt-Väisälä frequency* N_c^2 in case of constant adiabatic and equilibrium sound speeds becomes negative, implying $v_c < v_{eq}$. However, since this is not a sufficient condition, other physical affects play a crucial role (such as *fluid stratification* quantified by K_s in our case) in damping the perturbations even when the system appears to be energetically unstable. When $v_c > v_{eq}$ (i.e. positive N_c^2), higher extent of stratification in the fluid acts as a further catalyst to the process of damping of the induced perturbations from the glitch. On the other hand, when the extent of stratification is small and unable to compensate for a large negative difference between v_c and v_{eq} (i.e. large negative N_c^2), the perturbations grow exponentially as soon as they leave the limited stratified regions of the fluid. A very similar phenomenon takes place when the adiabatic and equilibrium sound speeds are allowed to vary in spatial coordinates although the mathematical intricacies are a lot more complex and not very straightforward. We defer the complete and detailed exploration of this affect (in case $\partial_z v_c \neq 0$) for future work keeping in mind that growing modes are a possible case of interest for systems that are energetically unstable, such as accretion systems.

6 Conclusions

To conclude our study, one can broadly make the following reiterations and conclusions. We have extended the previous works by van Eysden and Melatos [26] and Bennett et al. [7], by incorporating more general *equation of state* (characterized by v_c) and *stratification length* (characterized by K_s) in sections 2 and 3. We then derived the expected time-scales of emission of gravitational wave signals and the corresponding strain magnitudes from mass-quadrupole and current-quadrupole formalisms in section 4. In order to better visualize the results, we explored the signal characteristics in N^2 and v_c^o parameter space by making some relevant approximations given by (81) in section 4.3. The results are shown in figure 4, where we find that it is

possible for such a hydrodynamic system to produce gravitational waves at a ground-based detector with a strain of order greater than $O(10^{-25})$ for a source at a distance of roughly 1 kpc. The corresponding time-scales for the loudest signals are as long as $O(300)$ days. The results in figure 4 are explored for favorable end of physical parameters such as at glitch magnitude $\epsilon = O(10^{-4})$, $d_{\text{source}} = 1\,\text{kpc}$ and $f = 100\,\text{Hz}$. The analysis yields a strain magnitude as high as $O(10^{-21})$ in the very near and thin vicinity of low ranges of N^2 less than $O(10^{-5})$, and v_{c}^{o} in the range of $0.09c$ to $0.11c$ for most of the signal polarizations. Yet, for a more general and broader range of values of the aforementioned parameters, one can expect emission of the order of $O(10^1 - 10^{1.5})$ days in duration with a strength of $O(10^{-23.5} - 10^{-26.5})$. It must be noted that the current-quadrupole contribution tends to be larger than the corresponding mass-quadrupole contribution to the emitted signal which is evident in the results in section 4 and figure 4. This is mostly because of the characteristic amplitude h_{o}^{C} being larger than h_{o}^{M} by a factor[18] of $\frac{2g}{3\Omega c}$. Furthermore, the lower ranges of N^2 (i.e. as low as $10^{-6} - 10^{-7}$) are debatable and somewhat physically unexplained. It must be noted that the classical *Brunt-Väisälä frequency* N_{c}^2 is expected to lie in the range of (0.01, 1) [26]. The equivalent magnitude of the lower end of the range of redefined *Brunt-Väisälä frequency* N^2 is then given by: $\mathsf{N}^2 \equiv \eta_{\text{o}}\mathsf{N}_{\text{c}}^2 \rightarrow 10^{-4}$, for $v_{\text{c}}^{\text{o}} = 0.1c$. Thus, very low values of N^2 lie outside of the current estimates on equivalent values of N_{c}^2. In fact, very loud signals of amplitude $O(10^{-25})$ and higher lie toward the thin lower end of current estimates on N_{c}^2 i.e. in the range of around $10^{-4} - 10^{-7}$ for N^2. Yet, the value of *Ekman number* E is expected to lie in the range of $10^{-17} - 10^{-7}$[26, 7, 8, 6, 3, 14, 4, 11, 16], whereas we have based all our analysis at $\mathsf{E} = 10^{-7}$ i.e. at higher viscosity. Moreover, the time-scales and corresponding gravitational wave emission depend on E such that, $\mathsf{E} \downarrow \equiv t_{\alpha\gamma} \uparrow \equiv h \uparrow$. Thus, at lower values of E, stronger emissions occur at higher values of N^2. This effect is shown in figure 7 where we have regenerated parts of figure 4 for $\mathsf{E} = 10^{-14}$.

Moreover, we can also derive characteristics of emitted signals as a function of rotational frequency f of the neutron star. It has been shown that the minimum strain amplitude $h_{\text{o}}^{\text{min}}$ of a continuous gravitational wave detectable by a network of 2 detectors searched over a large parameter space with a coherent search duration of T_{obs} hours during which the signal is present is given by [1]

$$h_{\text{o}}^{\text{min}}(\omega) = \mathsf{K}_t \left[\frac{\mathsf{S}_h(\omega)}{\mathsf{T}_{\text{obs}}(\omega)}\right]^{\frac{1}{2}} \tag{83}$$

where, $\sqrt{\mathsf{S}_h(\omega)}$ is the *multi-detector amplitude spectral density* for a network of 2 detectors (H1, L1), and K_t is roughly equal to 30. Given this relation, we can compare the strength of emitted gravitational wave signals with the detectable strain by aLIGO. We will again concern ourselves with emission at resonant frequencies only i.e. $\omega = \omega_{\text{R}}$. Moreover, we can express $h_{\text{o}}^{\text{min}}$ as a function of f instead of ω since ω_{R} is an implicit function of f. This allows us to rewrite as follows

$$h_{\text{o}}^{\text{min}}(f) \equiv 30.0 \left[\frac{\mathsf{S}_h(f)}{t_{\alpha\gamma}(f)}\right]^{\frac{1}{2}} \tag{84}$$

In figure 8, we plot $h_{\text{o}}^{\text{min}}(f)$ and compare it with the emitted gravitational wave amplitudes as a function of f[19]. We have set the parameters E, v_{c}^{o} and N^2 to nominal values of 10^{-10}, $0.1c$ and 10^{-4} respectively following the discussion in the previous paragraphs. We find that for such a selected region in parameters space in 8, it is possible to detect such emissions with current aLIGO sensitivity, especially in the mid to high frequency range.

One must be careful in interpreting that we have assumed a spatially and temporally invariant N^2 in order to simplify our results for easier graphical and parametric visualization. In principle, one could vary all parameters (i.e. N^2 or K_{s}, v_{c}, v_{eq}) in all possible manners since all underlying analytically derived results in sections 2-4.2 are general in nature and assume none of the approximations described in section 4.3. More importantly, the main aim of this study was to estimate the strength of the emitted signals and their time-scales as a function of spatial variation in the adiabatic sound speed v_{c} and stratification length characterized by K_{s} (or, v_{c}). This is revealed in full detail in the figure 4 and figure 5. It is found that signal characteristics are quite sensitive to small spatial variations in v_{c} and K_{s}. In fact, the effective time-scales increase by a factor of 300 when $\partial_z v_{\text{c}} = -10^{-4}$ compared to when $\partial_z v_{\text{c}} = 0$. The corresponding emitted signal strengths also increase by a proportional magnitude as seen in figure 4, 5.

There are certain aspects that we have overlooked, such as the inclusion of magnetic field to the system. The strong magnetic field in neutron stars affect the crust-core interactions and coupling dynamics of the super-fluid [28], possibly affecting the boundary conditions for the system. Recent works by van Eysden [25] have explored the effect of magnetic field on post-glitch relaxation phase. In conclusion, we believe this to be a viable model to predict the expected order of magnitude and approximate characteristics of the emitted gravitational wave signals. It lays down a basic approach to predict the approximate internal state of the neutron star and first-order variations in it, if any such transient signal is detected by gravitational wave detectors from a neutron star undergoing post-glitch relaxation phase.

[18] This factor yields a value of the order of $O(10^1 - 10^2)$ for a neutron star rotating with a frequency of the order of $O(10^2)$ Hz, assuming $g = O(10^{12})$.

[19] Note that $t_{\alpha\gamma}$ is expressed in hours. Refer to section **A.7** in ***Appendix* A** for more details on the subject.

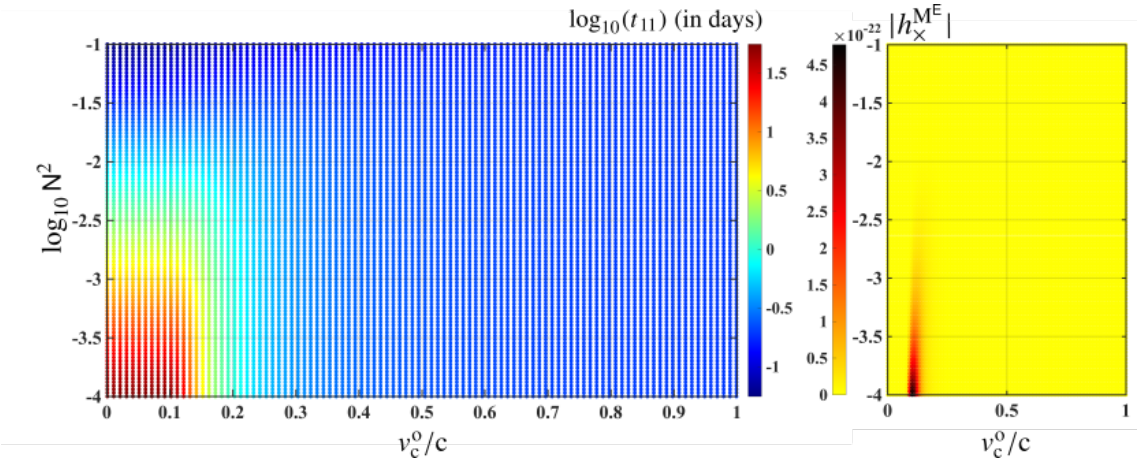

Figure 7: Sensitivity to E: The characteristics of emitted signals for $\mathsf{E} = 10^{-14}$ and $\partial_{\tilde{z}} v_{\mathrm{c}} = 0$ are shown, while setting $f = 100\,\mathrm{Hz}$, $\epsilon = 10^{-4}$, $d_{\mathrm{source}} = 1\,\mathrm{kpc}$, $\mathsf{L} = 10^4\mathrm{m}$, $g = 10^{12}\mathrm{m/sec^2}$, $\rho_{\mathrm{o}} = 10^{17}\mathrm{Kg/m^3}$. Note the possible emission of loud amplitudes within the range of $\mathsf{N}^2 \in (10^{-4}, 10^{-1})$; the equivalent classical *Brunt-Väisälä frequency* $\mathsf{N}^2_{\mathrm{c}}$ for this range lies within permitted physical expectations.

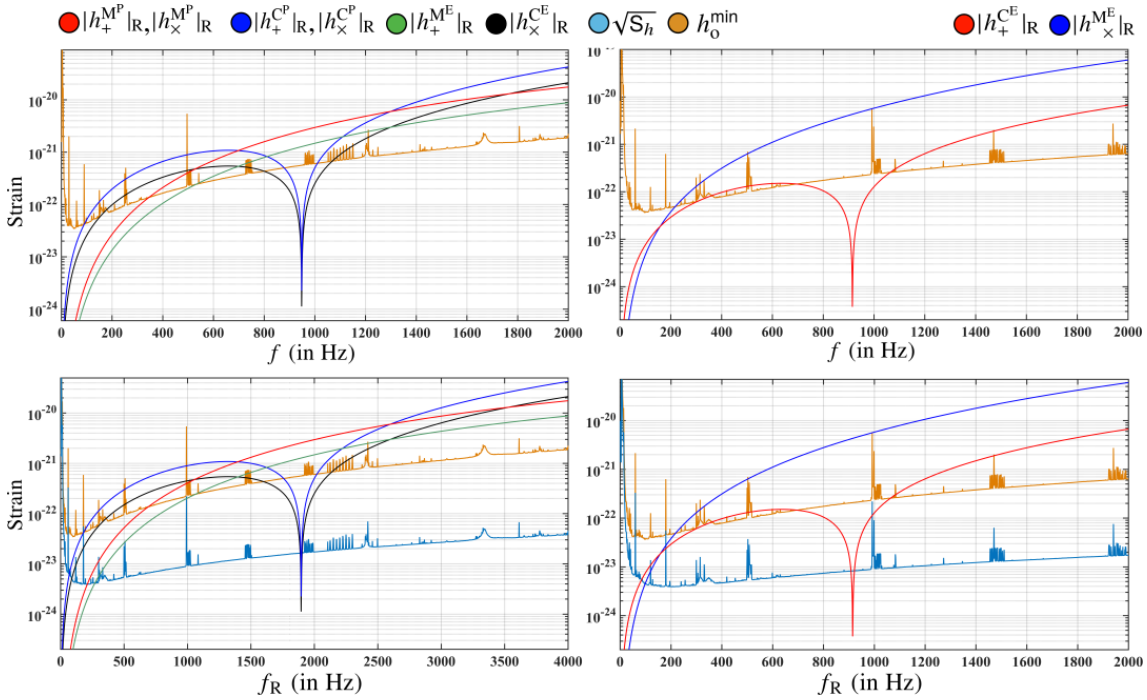

Figure 8: Sensitivity vs. f: The characteristics of emitted signals[20] as well as $h^{\mathrm{min}}_{\mathrm{o}}$ are shown as function of neutron star's rotational frequency f as well as the emitted resonant frequency f_{R}, given by $f_{\mathrm{R}} = \omega_{\mathrm{R}}/2\pi$. We have set $v^{\mathrm{o}}_{\mathrm{c}} = 0.1c$, $\mathsf{N}^2 = 10^{-4}$, $\mathsf{E} = 10^{-10}$, $\epsilon = 10^{-4}$, $d_{\mathrm{source}} = 1\,\mathrm{kpc}$, $\mathsf{L} = 10^4\mathrm{m}$, $g = 10^{12}\mathrm{m/sec^2}$, $\rho_{\mathrm{o}} = 10^{17}\mathrm{Kg/m^3}$, $\partial_{\tilde{z}} v_{\mathrm{c}} = 0$. Note that the emitted amplitudes are largely insensitive to $\partial_{\tilde{z}} v_{\mathrm{c}}$ for the chosen points in $\{v^{\mathrm{o}}_{\mathrm{c}}, \mathsf{N}^2\}$ parameter space. The *multi-detector amplitude spectral density* $\sqrt{\mathsf{S}_h(\omega)}$ is calculated by taking the harmonic mean of the individual amplitude spectral densities of H1 (aLIGO Hanford) and L1 detectors (aLIGO Livingston) measured during initial days of the O1 run i.e. Sept 12 – Oct 20, 2015.

7 Acknowledgments

I would like to extend my hearty thanks to Maria Alessandra Papa at the Max-Planck-Institut für Gravitationphysik for her support throughout, and to Andrew Melatos for his input through the course of this work.

[20] Note that the resonant frequencies of emission for different contributions (mass and current-quadrupole), for a given orientation of the observer (polar, equatorial, or otherwise), depend on individual constituent polarizations (+ and ×), which in turn depend on different featuring time-scales ($t_{\alpha\gamma}$), as seen in figure 4 and section 4. The overall signal is a superposition of all such individual emissions shown in figure 8, possibly at multiple resonant frequencies for a single source with a given orientation. In this regard, (84) assumes that these individual emissions are resolvable in frequency; this usually holds true when the featuring time-scales $t_{\alpha\gamma}$ are not very small (see 4.1, 4.2).

A Appendix

A.1 Time-evolution

In this section, we derive the time-evolution of the $\chi(r,\phi,z,t)$ function. We begin by separating the time-dependence in $\chi(r,\phi,z,t)$ by separating the variables,

$$\chi(r,\phi,z,t) \equiv \bar{\chi}(r,\phi,z)\mathsf{T}(t) \tag{A.1.1}$$

We can then take the time-derivative of (42)

$$\partial_t(\delta v_z)|_{z=\pm1} = \mp\frac{1}{2}\mathsf{E}^{\frac{1}{2}}\partial_t(\vec{\nabla}\times\delta\vec{v})_z|_{z=\pm1} = \pm\frac{1}{2}\mathsf{E}^{\frac{1}{2}}\left[\frac{1}{r}\frac{\partial}{\partial r}(r\partial_t[\delta v_\phi]) - \frac{1}{r}\frac{\partial}{\partial\phi}(\partial_t[\delta v_r])\right]\Bigg|_{z=\pm1} \tag{A.1.2}$$

Ignoring all the $O(\mathsf{E}^1)$ or higher order terms on the right-hand side and using results from sections 3.4, 3.5 and (44), we get

$$\partial_t[\delta v_z^{(1)}]|_{z=\pm1} = \mp\frac{1}{4\mathsf{F}}\left[\frac{1}{r^2}\frac{\partial^2\chi}{\partial\phi^2} + \frac{1}{r}\frac{\partial}{\partial r}(r\frac{\partial\chi}{\partial r})\right]\Bigg|_{z=\pm1} = \pm\frac{1}{4\mathsf{F}}\lambda_{\alpha\gamma}^2\chi|_{z=\pm1} \tag{A.1.3}$$

Moreover, we use (39) to re-write the previous expression as

$$\left[\frac{\eta(z)}{\mathsf{FN}^2(z)}\frac{\partial\dot{\chi}}{\partial z} + \left\{\frac{-\partial_z\eta}{\mathsf{FN}^2(z)} - 1\right\}\dot{\chi}\right]\Bigg|_{z=\pm1} = \mp\frac{1}{4\mathsf{F}}\lambda_{\alpha\gamma}^2\chi|_{z=\pm1} \tag{A.1.4}$$

Since, we have separated the time variable from the rest of the spatial coordinates, we may further re-write the above as

$$\left[\frac{\eta(z)}{\mathsf{FN}^2(z)}\frac{\partial\bar{\chi}}{\partial z} + \left\{\frac{-\partial_z\eta}{\mathsf{FN}^2(z)} - 1\right\}\bar{\chi}\right]\Bigg|_{z=\pm1}\dot{\mathsf{T}}(t) = \mp\frac{1}{4\mathsf{F}}\lambda_{\alpha\gamma}^2\bar{\chi}|_{z=\pm1}\mathsf{T}(t) \tag{A.1.5}$$

Moreover, we further reduce the above equation by separating the variables into (r,ϕ) and z to

$$\left[\frac{\eta(\pm1)}{\mathsf{FN}^2(\pm1)}\frac{\partial\mathsf{Z}_{\alpha\gamma}}{\partial z}\Bigg|_{z=\pm1} + \left\{\frac{-\partial_z\eta|_{z=\pm1}}{\mathsf{FN}^2(\pm1)} - 1\right\}\times \mathsf{Z}_{\alpha\gamma}(\pm1)\right]\dot{\mathsf{T}}(t) = \mp\frac{1}{4\mathsf{F}}\lambda_{\alpha\gamma}^2\mathsf{Z}_{\alpha\gamma}(\pm1)\mathsf{T}(t) \tag{A.1.6}$$

The equation above can now be solved to yield $\mathsf{T}(t)$,

$$\mathsf{T}(t) \propto e^{-\omega_{\alpha\gamma}t} \tag{A.1.7}$$

such that $\omega_{\alpha\gamma}$ is given by

$$\omega_{\alpha\gamma} = \frac{1}{4\mathsf{F}}\lambda_{\alpha\gamma}^2\mathsf{Z}_{\alpha\gamma}(1)\left[\frac{\eta(1)}{\mathsf{FN}^2(1)}\frac{\partial\mathsf{Z}_{\alpha\gamma}}{\partial z}\Bigg|_{z=1} + \left\{\frac{-\partial_z\eta|_{z=1}}{\mathsf{FN}^2(1)} - 1\right\}\mathsf{Z}_{\alpha\gamma}(1)\right]^{-1} \tag{A.1.8}$$

Note that $\mathsf{Z}_{\alpha\gamma}(z)$ is symmetric about $z=0$ plane and we have evaluated the expression at $z=1$.

A.2 Bessel-Fourier Coefficients

In this section, we will calculate the *Bessel-Fourier coefficients* introduced in (52) in detail. We will use the *orthogonality property* of the Bessel functions, which states that Bessel functions are orthogonal with respect to the inner product as follows[21]

$$\langle\mathsf{J}_\alpha(\lambda_{\alpha\gamma}r),\mathsf{J}_\alpha(\lambda_{\alpha\alpha}r)\rangle = \int_0^1 r\,\mathsf{J}_\alpha(\lambda_{\alpha\gamma}r)\mathsf{J}_\alpha(\lambda_{\alpha\alpha}r)\mathrm{d}r = \frac{1}{2}\delta_{\gamma\alpha}[\mathsf{J}_{\alpha+1}(\lambda_{\alpha\gamma}r)]^2 \tag{A.2.1}$$

Now, for a Fourier-Bessel series of the form $f(r) = \sum_{\alpha=1}^{\infty}\mathsf{C}_\alpha\mathsf{J}_\alpha(\lambda_{\alpha\alpha}r)$, the coefficients C_α can be calculated by taking projection of the function $f(r)$ over the corresponding Bessel functions,

$$\mathsf{C}_\alpha = \frac{\langle f(r),\mathsf{J}_\alpha(\lambda_{\alpha\alpha}r)\rangle}{\langle\mathsf{J}_\alpha(\lambda_{\alpha\gamma}r),\mathsf{J}_\alpha(\lambda_{\alpha\gamma}r)\rangle} \tag{A.2.2}$$

Using the above relation in combination with (53), we can substitute for $f(r)$,

$$f(r) = \delta\mathsf{P}_0 - \delta\mathsf{P}_\infty = \sum_{\alpha=0}^{\infty}\sum_{\gamma=1}^{\infty}\omega_{\alpha\gamma}^{-1}\mathsf{J}_\alpha(\lambda_{\alpha\gamma}r)\times [\mathsf{A}_{\alpha\gamma}\mathsf{Cos}(\alpha\phi) + \mathsf{B}_{\alpha\gamma}\mathsf{Sin}(\alpha\phi)]\mathsf{Z}_{\alpha\gamma}(z) = \sum_{\alpha=0}^{\infty}\mathsf{C}_\alpha r^\alpha(r^2-1)\,\mathsf{Cos}(\alpha\phi) \tag{A.2.3}$$

which, when applied to (A.2.2), gives

$$\omega_{\alpha\gamma}^{-1}\mathsf{A}_{\alpha\gamma}\mathsf{Cos}(\alpha\phi)\mathsf{Z}_{\alpha\gamma}(z) = \frac{2}{\mathsf{J}_{\alpha+1}^2(\lambda_{\alpha\gamma})}\int_0^1 r\times \mathsf{J}_\alpha(\lambda_{\alpha\gamma}r)[\delta\mathsf{P}_0 - \delta\mathsf{P}_\infty]\,\mathrm{d}r \tag{A.2.4}$$

We multiply both sides with $\mathsf{Cos}(\alpha\phi)$ and integrate the resulting expression in ϕ and z variables assuming that $\mathsf{A}_{\alpha\gamma}$ is an absolute constant, and arrive at the following result,

$$\mathsf{A}_{\alpha\gamma} = \frac{2\omega_{\alpha\gamma}}{\pi\mathsf{J}_{\alpha+1}^2(\lambda_{\alpha\gamma})}\int_0^{2\pi}\mathrm{d}\phi\int_0^1\mathrm{d}z\int_0^1 r\,\mathrm{d}r\times \mathsf{J}_\alpha(\lambda_{\alpha\gamma}r)\,\mathsf{Cos}(\alpha\phi)\,[\delta\mathsf{P}_0 - \delta\mathsf{P}_\infty]\,\mathsf{Z}_{\alpha\gamma}^{-1}(z) \tag{A.2.5}$$

Similarly, for $\mathsf{B}_{\alpha\gamma}$,

$$\mathsf{B}_{\alpha\gamma} = \frac{2\omega_{\alpha\gamma}}{\pi\mathsf{J}_{\alpha+1}^2(\lambda_{\alpha\gamma})}\int_0^{2\pi}\mathrm{d}\phi\int_0^1\mathrm{d}z\int_0^1 r\,\mathrm{d}r\times \mathsf{J}_\alpha(\lambda_{\alpha\gamma}r)\,\mathsf{Sin}(\alpha\phi)\,[\delta\mathsf{P}_0 - \delta\mathsf{P}_\infty]\,\mathsf{Z}_{\alpha\gamma}^{-1}(z) \tag{A.2.6}$$

[21] $\delta_{\gamma\alpha}$ is the *Dirac-delta function*.

A.3 Quadrupole moment formalism

In this section, we will underline the formalism for calculating the expressions (62)-(71) for gravitational wave emission. In the reference frame of a *polar observer* at a distance d, the components of the gravitational wave strain in Einstein's quadrupole moment formalism in the transverse traceless gauge (abbreviated as 'TT') are given by

$$h_+(t) = h^{\rm TT}_{xx}(t) = -h^{\rm TT}_{yy}(t) = \frac{\rm G}{c^4 d}[\ddot{\rm I}_{xx}(t) - \ddot{\rm I}_{yy}(t)] \tag{A.3.1}$$

$$h_\times(t) = h^{\rm TT}_{xy}(t) = \frac{2\rm G}{c^4 d}\ddot{\rm I}_{xy}(t) \tag{A.3.2}$$

where, $\rm I_{ik}(t)$ is the reduced quadrupole moment of inertia, and is given in terms of stress-energy tensor component $\rm T^{00}$ by,

$$\rm I_{ik}(t) = \frac{1}{c^2}\int d^3\vec{x}\left[x_i x_k - \delta_{ik}\frac{|\vec{x}|^2}{3}\right]T^{00}(\vec{x},t) \tag{A.3.3}$$

Now, combining (A.3.1), (A.3.2) and (A.3.3), we get

$$h^{\rm P}_+(t) = \frac{\rm G}{c^6 d}\int d^3\vec{x}[x^2-y^2]\ddot{\rm T}^{00}(\vec{x},t) = \frac{\rm G}{c^6 d}\int d^3\vec{r}\, r^2 {\rm Cos}(2\phi)\ddot{\rm T}^{00}_{\rm NA}(\vec{r},t) \tag{A.3.4}$$

$$h^{\rm P}_\times(t) = \frac{2\rm G}{c^6 d}\int d^3\vec{x}[xy]\ddot{\rm T}^{00}(\vec{x},t) = \frac{\rm G}{c^6 d}\int d^3\vec{r}\, r^2 {\rm Sin}(2\phi)\ddot{\rm T}^{00}_{\rm NA}(\vec{x},t) \tag{A.3.5}$$

where, the sub-script NA refers to non-axisymmetric terms. Moreover, in case of a perfect fluid [neglecting viscous terms while evaluating $\rm T^{\mu\nu}$ since they are of the order $O(\rm E)$], the stress-energy tensor component $\rm T^{00}$ is given by

$$\rm T^{00} = \left[\rho + \frac{p}{c^2}\right]u^0 u^0 + p g^{00} \tag{A.3.6}$$

where, the 0-component u^0 of the 4-velocity $\vec{u}$ is given by

$$u^0 = \frac{c}{\sqrt{1-\frac{\vec{v}\cdot\vec{v}}{c^2}}} \tag{A.3.7}$$

We break the expression (A.3.6) into separate terms describing the constitutive equilibrium and perturbative terms, i.e. $\rho \to \rho_e + \epsilon\delta\rho$, $p \to p_e + \epsilon\delta p$ and $\vec{v} \to \vec{v}_r + \delta\vec{v}$, as described in section 3.2. Here, $\vec{v}_r$ is simply the velocity of a fluid element given in cylindrical coordinates by $\vec{v}_r = (0, \Omega r, 0)$, assuming co-rotation with the neutron star crust. Note that equilibrium state is axisymmetric in nature and doesn't contribute to the signal emission. The contributing non-axisymmetric terms in $\rm T^{00}$ are then given by[22]

$$\begin{aligned}\rm T^{00}_{NA} = \epsilon\delta\rho c^2 + (\rho_e c^2 + p_e)\left[2\frac{\delta\vec{v}\cdot\vec{v}_r}{c^2} + \frac{\delta\vec{v}\cdot\delta\vec{v}}{c^2}\right] + \\ \epsilon(\delta\rho c^2 + \delta p)\left[2\frac{\delta\vec{v}\cdot\vec{v}_r}{c^2} + \frac{\vec{v}_r\cdot\vec{v}_r}{c^2} + \frac{\delta\vec{v}\cdot\delta\vec{v}}{c^2}\right] \equiv \\ \epsilon\delta\rho c^2 + (\rho_e c^2 + p_e)\left[2\frac{\delta\vec{v}\cdot\vec{v}_r}{c^2} + \frac{\delta\vec{v}\cdot\delta\vec{v}}{c^2}\right] + \\ (\epsilon\delta\rho c^2 + \delta p)\left[\frac{\vec{v}_r\cdot\vec{v}_r}{c^2}\right]\end{aligned} \tag{A.3.8}$$

Note that there exists no explicit factor of ϵ when it comes to $\delta\vec{v}$ as discussed previously in section 3.2. The factor of ϵ in the order of magnitude of $\delta\vec{v}$ is implicitly contained within $\delta\vec{v}$. Further, combining the expressions (A.3.4), (A.3.5) and (A.3.8), we calculate the gravitational wave emission up to the order $O(\epsilon^1)$ given by (62)-(71).

A.4 Current-quadrupole moment

In this section, we briefly describe the method to derive strain amplitude for the current-quadrupole contribution quoted in (72)-(76). We follow [24, 17, 7], and make appropriate modifications corresponding to our assumption of varying stratification length and adiabatic sound speed. The general expression for the + and × polarizations contributed by the current-quadrupole moment (labeled by the super-script C) for a general observer at distance d is given by [7, 17, 24],

$$h^{\rm C}_+(t) = \frac{\rm G}{2c^5 d}\left[\frac{5}{2\pi}\right]^{\frac{1}{2}}[{\rm Im}\{\dddot{\rm C}^{21}(t)\}{\rm Sin}(i) + {\rm Im}\{\dddot{\rm C}^{22}(t)\}{\rm Cos}(i)] \tag{A.4.1}$$

$$h^{\rm C}_\times(t) = \frac{\rm G}{4c^5 d}\left[\frac{5}{2\pi}\right]^{\frac{1}{2}}[{\rm Re}\{\dddot{\rm C}^{21}(t)\}{\rm Sin}(2i) + {\rm Re}\{\dddot{\rm C}^{22}(t)\}\,[1+{\rm Cos}^2(i)]] \tag{A.4.2}$$

where, $\rm C^{l\nu}(t)$ are the (l,ν)-multipoles of the mass-current distribution. Note that we have only considered the leading order quadrupole moment ($l = 2$), which is the lowest multipole moment that contributes to the gravitational wave emission via its non-vanishing second-order time-derivative $\dddot{\rm C}^{2\nu}(t)$. The presence of additional c^5 factor, as opposed to c^4 in case of the mass-quadropole moment, suggests that the current-quadrupole contribution is much smaller than the mass-quadrupole moment. This is true for systems with low density; for high-density systems such as a neutron star, current-quadrupole emission may be larger than mass-quadrupole contribution, as described in section 4.2. We have also ignored the $\nu = 0$ mode which contributes at the order of $O(\rm E^1)$ while retaining the more significant

[22] Here, we have assumed $g^{00} = -1$ and $|v^2| \ll c^2$.

$\nu = 1, 2$ modes. Moreover, i denotes the angle between neutron star's rotation axis with respect to observer's line of sight; $i = 0$ for a polar observer, and $i = 90°$ for an equatorial observer. The $C^{2\nu}(t)$ are explicitly given by [7][23]

$$C^{2\nu}(t) = \frac{(-1)^{\nu+1} 8\pi (10\pi)^{\frac{1}{2}}}{15\nu\, \rho_o^{-1} L^{-6} (\delta\Omega)^{-1}} \sum_{\gamma=1}^{\infty} V_{\nu\gamma} e^{-(E^{\frac{1}{2}}\omega_{\nu\gamma} + i\nu)\Omega t} \tag{A.4.3}$$

where

$$V_{\nu\gamma} = 2A_{\nu\gamma}\omega_{\nu\gamma}^{-1} \int_0^1 dr \int_0^1 dz\, r^{\nu+1} z^{2-\nu} \times \hat{U}\Big[J_\nu(\lambda_{\nu\gamma} r) Z_{\nu\gamma}(z) \rho_e(z)\Big] \tag{A.4.4}$$

Moreover, the operator $\hat{U}$ is written as

$$\hat{U} = \left[z\frac{\partial^2}{\partial r^2} + \frac{z}{r}\frac{\partial}{\partial r} - z\frac{\nu^2}{r^2} - r\frac{\partial^2}{\partial r \partial z}\right] + 2F\left[r^2\frac{\partial^2}{\partial z^2} - rz\frac{\partial^2}{\partial r \partial z} - 2z\frac{\partial}{\partial z}\right] \tag{A.4.5}$$

Finally, the expressions for + and × polarizations can now be reduced using the above relations to the expressions quoted in (72)-(76).

A.5 $\kappa_{\nu\gamma}$ and $V_{\nu\gamma}$

In this section, we quote the full expression of $\kappa_{\nu\gamma}$[24].

$$\kappa_{\nu\gamma} = 2\omega_{\nu\gamma}^{-1} A_{\nu\gamma}\Bigg[\int_0^1 dr\, r^3 J_\nu(\lambda_{\nu\gamma} r) \int_0^1 dz\, \partial_z[-Z_{\nu\gamma}(z)\rho_e(z)] + K\int_0^1 dr\, r^4 \partial_r[J_\nu(\lambda_{\nu\gamma} r)] \times \int_0^L dz \left[1 + \frac{K}{K_s(z)}\right] Z_{\nu\gamma}(z)\rho_e(z) + \frac{\Omega^2 L^2}{c^2}\int_0^1 dr\, r^5 J_\nu(\lambda_{\nu\gamma} r) \times \int_0^1 dz \Big[\partial_z[-Z_{\nu\gamma}(z)\rho_e(z)] + K Z_{\nu\gamma}(z)\rho_e(z)\Big]\Bigg] \tag{A.5.1}$$

Moreover, following the assumptions described in (81) in section 5, the above expression for $\kappa_{\nu\gamma}$ can be further reduced to a simpler and easier form. The simplifying assumptions lead to the case where all coefficients in (46) become effectively and approximately invariant with respect to the z-coordinate; this leaves the solution for $Z_{\nu\gamma}(z)$ straightforward to achieve. Moreover, the integrals in exponentials involving K_s in (A.5.1) are dissolved, and the resulting exponential terms can be folded into $Z_{\nu\gamma}(z)$ to yield

$$\kappa_{\nu\gamma} = 2\omega_{\nu\gamma}^{-1} A_{\nu\gamma}\Bigg[\mathcal{L}_1 \int_0^1 dr\, r^3 J_\nu(\lambda_{\nu\gamma} r) + K\left[1 + \frac{K}{K_s}\right]\mathcal{L}_2 \int_0^1 dr\, r^4 \partial_r[J_\nu(\lambda_{\nu\gamma} r)] + \frac{\Omega^2 L^2}{c^2}\Big[\mathcal{L}_1 + K\mathcal{L}_2\Big]\int_0^1 dr\, r^5 J_\nu(\lambda_{\nu\gamma} r)\Bigg] \tag{A.5.2}$$

where, $\mathcal{L}_1$ and $\mathcal{L}_2$ are given in terms of $\mathcal{K}_\pm$

$$\mathcal{L}_1 = \frac{(FN^2 - \mathcal{K}_-)[1 - e^{-\mathcal{K}_-}] - (FN^2 - \mathcal{K}_+)[1 - e^{-\mathcal{K}_+}]}{(FN^2 - \mathcal{K}_-)e^{\mathcal{K}_+} - (FN^2 - \mathcal{K}_+)e^{\mathcal{K}_-}} \tag{A.5.3}$$

$$\mathcal{L}_2 = \frac{(FN^2 - \mathcal{K}_-)\frac{1 - e^{-\mathcal{K}_-}}{\mathcal{K}_-} - (FN^2 - \mathcal{K}_+)\frac{1 - e^{-\mathcal{K}_+}}{\mathcal{K}_+}}{(FN^2 - \mathcal{K}_-)e^{\mathcal{K}_+} - (FN^2 - \mathcal{K}_+)e^{\mathcal{K}_-}} \tag{A.5.4}$$

Further, $\mathcal{K}_\pm$ in (A.5.3) and (A.5.4) is given by

$$\mathcal{K}_\pm = \frac{1}{2}[K_s \pm (K_s^2 + \eta_o^{-1}[N^2\lambda_{\nu\gamma}^2 + \partial_z\eta - \partial_z^2\eta])^{\frac{1}{2}}] \tag{A.5.5}$$

where, $\eta_o = (v_c^o/c)^2$, $\partial_z\eta \to 2v_c^o\partial_z v_c$ and $\partial_z^2\eta \to 2(\partial_z v_c)^2$. Similarly, one could arrive at the reduced expression for $V_{\nu\gamma}$ in terms of $\mathcal{L}_3^{(g)}$, $\mathcal{L}_4^{(g)}$ and $\mathcal{L}_5^{(g)}$. We define $\mathcal{L}_3^{(g)}$, $\mathcal{L}_4^{(g)}$ and $\mathcal{L}_5^{(g)}$ as follows

$$\mathcal{L}_3^{(g)} = \frac{(FN^2 - \mathcal{K}_-)\mathcal{H}_g(\mathcal{K}_-) - (FN^2 - \mathcal{K}_+)\mathcal{H}_g(\mathcal{K}_-)}{(FN^2 - \mathcal{K}_-)e^{\mathcal{K}_+} - (FN^2 - \mathcal{K}_+)e^{\mathcal{K}_-}} \tag{A.5.6}$$

$$\mathcal{L}_4^{(g)} = \frac{(FN^2 - \mathcal{K}_-)\frac{\mathcal{H}_g(\mathcal{K}_-)}{\mathcal{K}_-^{-1}} - (FN^2 - \mathcal{K}_+)\frac{\mathcal{H}_g(\mathcal{K}_+)}{\mathcal{K}_+^{-1}}}{(FN^2 - \mathcal{K}_-)e^{\mathcal{K}_+} - (FN^2 - \mathcal{K}_+)e^{\mathcal{K}_-}} \tag{A.5.7}$$

$$\mathcal{L}_5^{(g)} = \frac{(FN^2 - \mathcal{K}_-)\frac{\mathcal{H}_g(\mathcal{K}_-)}{\mathcal{K}_-^{-2}} - (FN^2 - \mathcal{K}_+)\frac{\mathcal{H}_g(\mathcal{K}_+)}{\mathcal{K}_+^{-2}}}{(FN^2 - \mathcal{K}_-)e^{\mathcal{K}_+} - (FN^2 - \mathcal{K}_+)e^{\mathcal{K}_-}} \tag{A.5.8}$$

where, $\mathcal{H}_g(\mathcal{K}_-)$ is defined in terms of the integral given

[23] In case of current-quadrupole contribution, it is possible to have continuous emission of gravitational waves (at large time-scales, $t \gg t_{2\nu}$), as shown by Bennett et al. [7]. This continuous residual emission is not artificial (cf. van Eysden and Melatos [26]). In calculating the expression for $C^{2\nu}(t)$, we have ignored terms responsible for such residual continuous contribution since we concern ourselves solely with transient emission.

[24] The pre-factor of 2 in $\kappa_{\nu\gamma}$ comes from extending the symmetric integral to $z \in [-1, 1]$.

below[25]

$$\mathcal{H}_{\rm g}(\mathcal{K}_{\pm}) = \int_0^1 {\rm d}z\, z^{\rm g} e^{-\mathcal{K}_{\pm} z} \tag{A.5.9}$$

The resulting complete expression for $\mathsf{V}_{\nu\gamma}$ could then be expanded and written in terms of $\mathcal{L}_3^{(\rm g)}$, $\mathcal{L}_4^{(\rm g)}$ and $\mathcal{L}_5^{(\rm g)}$ as follows:

$$\mathsf{V}_{\nu\gamma} = 2\mathsf{A}_{\nu\gamma}\omega_{\nu\gamma}^{-1}\Big[\mathcal{L}_3^{(3-\nu)}\int_0^1 {\rm d}r\, r^{\nu-1}[r^2\partial_r^2[\mathsf{J}_\nu(\lambda_{\nu\gamma}r)] + r\partial_r[\mathsf{J}_\nu(\lambda_{\nu\gamma}r)] - \nu^2\mathsf{J}_\nu(\lambda_{\nu\gamma}r)] + \mathcal{L}_4^{(2-\nu)}\times$$
$$\int_0^1 {\rm d}r\, r^{\nu+2}\partial_r[\mathsf{J}_\nu(\lambda_{\nu\gamma}r)] + 2\mathsf{F}\Big[\mathcal{L}_5^{(2-\nu)}\int_0^1 {\rm d}r\, r^{\nu+3}\mathsf{J}_\nu(\lambda_{\nu\gamma}r) + \mathcal{L}_4^{(3-\nu)}\int_0^1 {\rm d}r\, r^{\nu+1}[r\partial_r[\mathsf{J}_\nu(\lambda_{\nu\gamma}r)] + 2\mathsf{J}_\nu(\lambda_{\nu\gamma}r)]\Big]\Big] \tag{A.5.10}$$

Moreover, the approximated expression of $t_{\nu\gamma}$ could also be calculated following (81), and is given by

$$t_{\nu\gamma} = \frac{4\mathsf{E}^{-\frac{1}{2}}\Omega^{-1}\mathsf{F}^2\mathsf{N}^2\Big[(\mathsf{FN}^2-\mathcal{K}_-)e^{\mathcal{K}_+} - (\mathsf{FN}^2-\mathcal{K}_+)e^{\mathcal{K}_-}\Big]}{\lambda_{\nu\gamma}^2\Big[(\eta_1\mathcal{K}_+ - \partial_z\eta|_{z=1} - \mathsf{FN}^2)(\mathsf{FN}^2-\mathcal{K}_-)e^{\mathcal{K}_+} - (\eta_1\mathcal{K}_- - \partial_z\eta|_{z=1} - \mathsf{FN}^2)(\mathsf{FN}^2-\mathcal{K}_+)e^{\mathcal{K}_-}\Big]} \tag{A.5.11}$$

where,

$$\eta_1 = \eta_{\rm o} + \partial_z\eta + \frac{1}{2}\partial_z^2\eta;\ \partial_z\eta|_{z=1} \to \partial_z\eta + \partial_z^2\eta$$

given,

$$\eta_{\rm o} = (v_{\rm c}^{\rm o}/c)^2,\ \partial_z\eta \to 2v_{\rm c}^{\rm o}\partial_z v_{\rm c} \text{ and } \partial_z^2\eta \to 2(\partial_z v_{\rm c})^2.$$

A.6 Error characterization

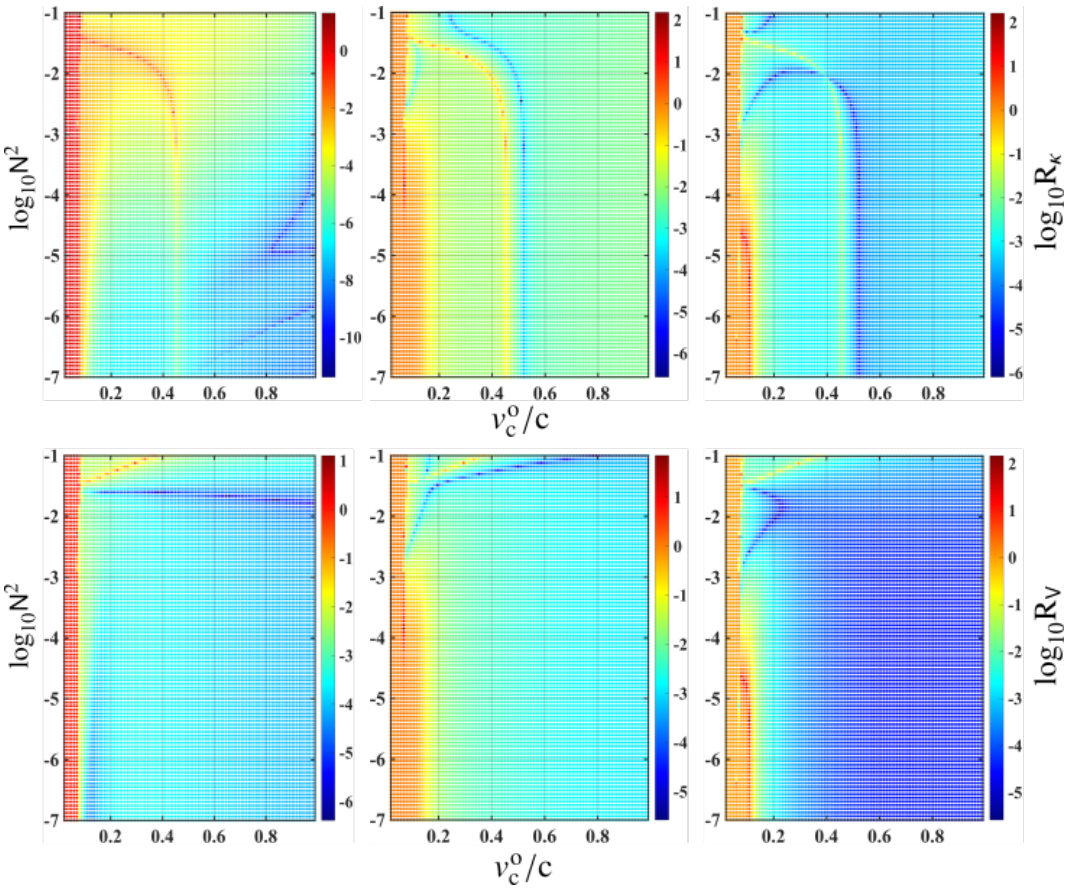

Figure 9: Error characteristics: 3 different set of data are plotted for the t_{21} mode at a rotational frequency of 100 Hz for a set of values of $\partial_z v_{\rm c}$ of $0c$, $10^{-3}c$ and $-10^{-4}c$ from left to right. Other relevant physical parameters are randomly chosen from astrophysical priors, as in all previous figures. The top panel represents R_κ while the bottom panel represents R_{V}. Note that larger values of R_κ and R_{V} signify large mismatch between approximated analytic and numerical results.

[25] It must be noted that the occurrences of (g) in expressions of $\mathcal{L}_3^{(\rm g)}$, $\mathcal{L}_3^{(\rm g)}$ and $\mathcal{L}_3^{(\rm g)}$ are intended as **super-scripts** and **not exponents**.

In this section, we show the comparison between analytically approximated and numerically computed results for $\kappa_{v\gamma}$ and $\mathsf{V}_{v\gamma}$. We have explored the results for the t_{21} mode since this is sufficient for our purposes. We define the differences between analytically approximated ($\kappa^{t}_{v\gamma}$, $\mathsf{V}^{t}_{v\gamma}$) and numerical ($\kappa^{n}_{v\gamma}$, $\mathsf{V}^{n}_{v\gamma}$) results as follows,

$$\mathsf{R}_{\kappa} = \left| \frac{\kappa^{t}_{v\gamma} - \kappa^{n}_{v\gamma}}{\kappa^{t}_{v\gamma} + \kappa^{n}_{v\gamma}} \right| \tag{A.6.1}$$

$$\mathsf{R}_{\mathsf{V}} = \left| \frac{\mathsf{V}^{t}_{v\gamma} - \mathsf{V}^{n}_{v\gamma}}{\mathsf{V}^{t}_{v\gamma} + \mathsf{V}^{n}_{v\gamma}} \right| \tag{A.6.2}$$

In figure 9, we plot the characteristics of R_{κ} and R_{V} for 3 cases, when $\partial_z v_c \in \{0, 10^{-3}c, -10^{-4}c\}$. Moreover, the leftmost panels lay a baseline mismatch between approximated analytical values and numerically calculated values of $\kappa_{v\gamma}$ and $\mathsf{V}_{v\gamma}$. Note that since $\partial_z v_c = 0$ for these two panels, in principle, the numerical and approximated analytical results should not have a high mismatch. However, the results deviate from accuracy for certain regions in parameter space, especially for lower values of v_c^o. The center and rightmost panels show similar characteristics. One interesting point to note is that the mismatch in $\kappa_{v\gamma}$ and $\mathsf{V}_{v\gamma}$ follow somewhat similar characteristics to the time-scales plotted in figure 4. The underlying reason is fairly straightforward: larger time-scales occur when K_s becomes large in magnitude; this large magnitude of K_s tends to throw off the numerical results from accuracy while the approximated analytical results continue to follow an accurate description. Note that the factor $\rho_e(z)$ in the expressions of $\kappa_{v\gamma}$ and $\mathsf{V}_{v\gamma}$ tends to fall increasingly rapidly with z from its large value ρ_o at $z = 0$ for large magnitudes of K_s[26]. It is also found that the numerical values of $\mathsf{Z}_{v\gamma}(z)$ tend to wander inaccurately and sporadically into negative domain from tolerance-induced numerical errors nearing $z = 0$. This small discrepancy between values calculated by numerical methods and approximate analytical expressions is amplified by the larger value of $\rho_e(z)$ nearing $z = 0$ when K_s is large, leading to a large mismatch. This affect is realized in figure 9 for the case of $\partial_z v_c = 0$ i.e. leftmost panels.

A.7 $t_{v\gamma}$ vs f

In this section, we elaborate on the characteristics of emitted signals as a function of neutron star's rotational frequency f. In figure 10, we plot the time-scales for {2,1} and {1,1} modes i.e. t_{21} and t_{11}, as a function of f. These time-scales have been calculated and implicitly included in the results via (84) in figure 8. We can conclude from figure 10 that these time-scales may span orders of magnitudes; for (84) to be a valid measure of minimum detectable strain for such signals, the observation time for the coherent search must be larger than these time-scales i.e. $\mathsf{T}_{obs} \geq t_{v\gamma}$.

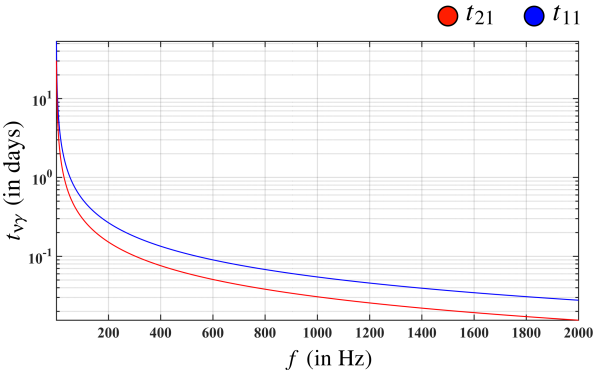

Figure 10: $t_{v\gamma}$ characteristics: t_{21} and t_{11} are plotted as a function of neutron star's rotational frequency f. We have set $v_c^o = 0.1c$, $\mathsf{N}^2 = 10^{-4}$, $\mathsf{E} = 10^{-10}$, $\epsilon = 10^{-4}$, $d_{source} = 1\,\text{kpc}$, $\mathsf{L} = 10^4\text{m}$, $g = 10^{12}\text{m/sec}^2$, $\rho_o = 10^{17}\text{Kg/m}^3$, $\partial_z v_c = 0$.

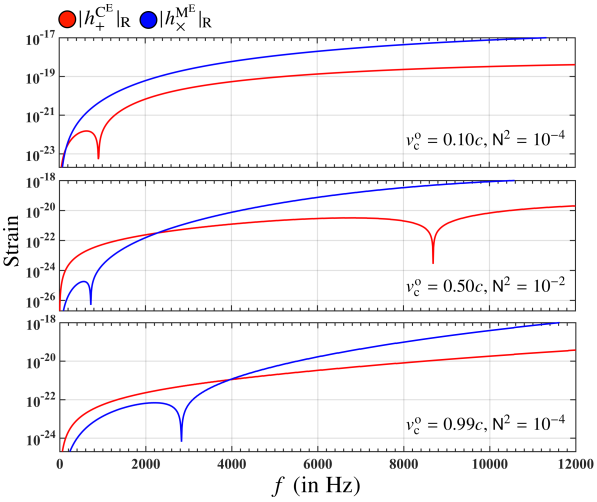

Figure 11: Emission characteristics: We have set $\mathsf{E} = 10^{-10}$, $\epsilon = 10^{-4}$, $d_{source} = 1\,\text{kpc}$, $\mathsf{L} = 10^4\text{m}$, $g = 10^{12}\text{m/sec}^2$, $\rho_o = 10^{17}\text{Kg/m}^3$, $\partial_z v_c = 0$. 3 different sets of values of v_c^o and N^2 are explored as shown. Note the appearance of dips in one or both the contributions in f-space i.e. mass-quadrupole and/or current-quadrupole emissions, due to variation in v_c^o and N^2.

Moreover, there is a noticeable dip in emission from current-quadrupole contribution in the mid-frequency range in figure 8. This dip is caused by $\mathsf{V}_{v\gamma}$ becoming negative with increasing frequency; the sharp dip occurs due to the inclusion of $\mathsf{V}_{v\gamma}$ in (72)-(75) via its absolute magnitude. This affect is not limited to $\mathsf{V}_{v\gamma}$ only i.e. current-quadrupole contribution. In fact, the presence of this dip in current-quadrupole and/or mass-quadrupole emission(s) depend upon the values of v_c^o and N^2. Like $\mathsf{V}_{v\gamma}$, $\kappa_{v\gamma}$ may also show similar effect for alternative values of v_c^o and/or N^2. Furthermore, the location of this dip in f-space is found to vary with v_c^o as

[26] While this effects the numerical results of $\kappa_{v\gamma}$ and $\mathsf{V}_{v\gamma}$, no such effect is present in the expression for time-scale $t_{v\gamma}$.

well as N^2. The location of this dip in f-space is also found to be less sensitive to variation in N^2 as compared to ν_c^o. In figure 11 above, we plot a part of figure 8 (top-right panel) to demonstrate the aforementioned effect.

References

[1] B Abbott *et al*. **Phys. Rev. D**, 76(8):082001, 2007.

[2] M Abney and R I Epstein. **J. Fluid Mech.**, 312 (1):327–340, 1996.

[3] A Adare *et al*. **PRL**, 98(17):172301, 2007.

[4] S S Adler *et al*. **PRL**, 91(18):182301, 2003.

[5] N Andersson, G L Comer, and R Prix. **Phys. Rev. Lett.**, 90(09):091101, 2003.

[6] N Andersson, G L Comer, and K Glampedakis. **Nuclear Phy. A**, 763(1):212–229, 2005.

[7] M F Bennett, C A van Eysden, and A Melatos. **MNRAS**, 409(4):1705–1718, 2010.

[8] C Cutler and L Lindblom. **ApJ**, 314(1):234–241, 1987.

[9] S Dall'Osso, G L Israel, L Stella, A Possenti, and E Perozzi. **ApJ**, 599(1):485–497, 2003.

[10] D I Jones and N Andersson. **MNRAS**, 331(3): 203–220, 2002.

[11] P K Kovtun, D T Son, and A O Starinets. **PRL**, 94(11):111601, 2005.

[12] A G Lyne, S L Shemar, and F Graham Smith. **MNRAS**, 315(3):534–542, 2000.

[13] A Mastrano and A Melatos. **MNRAS**, 361(3): 927–941, 2005.

[14] D Mateos, R C Myers, and R M Thomson. **PRL**, 98(10):101601, 2007.

[15] P M McCulloch, P A Hamilton, D McConnell, and E A King. **Nature**, 346(1):822–824, 1990.

[16] A Melatos and C Peralta. **ApJ**, 662(2):99–102, 2007.

[17] A Melatos and C Peralta. **ApJ**, 709(1):77, 2010.

[18] A Melatos, C Peralta, and J S B Wyithe. **ApJ**, 672 (2):1103–1118, 2008.

[19] J Mound and B Buffett. **J. Geophys. Res. (Solid Earth)**, 112(B5):5402, 2007.

[20] C Peralta, A Melatos, M Giacobello, and A Ooi. **ApJ**, 635(2):1224–1232, 2005.

[21] V Rezania and M Jahan-Miri. **MNRAS**, 315(2): 263–268, 2000.

[22] D M Sedrakian, M Benacquista, K M Shahabassian, A A Sadoyan, and M Hairapetyan. **Astrophysics**, 46(4):445–454, 2003.

[23] D M Sedrakian, M Benacquista, and K M Shahabassian. **Astrophysics**, 49(2):194–200, 2006.

[24] Kip S Thorne. **Reviews of Modern Physics**, 52 (2):299, 1980.

[25] C A van Eysden. **ApJ**, 789(2):142–155, 2014.

[26] C A van Eysden and A Melatos. **Class. Quantum Grav.**, 25(22):225020, 2008.

[27] C A van Eysden and A Melatos. **J. Fluid Mech.**, 729(1):180–213, 2013.

[28] M van Hoven and Y Levin. **MNRAS**, 410(2): 1036–1051, 2011.

[29] G Walin. **J. Fluid Mech.**, 36(2):289–307, 1969.

[30] M Yu, R N Manchester, G Hobbs, S Johnston, V M Kaspi, M Keith, A G Lyne, G J Qiao, V Ravi, J M Sarkissian, R Shannon, and R X Xu. **MNRAS**, 429(1):688–724, 2013.